Research Square

Preprints are preliminary reports that have not undergone peer review.
They should not be considered conclusive, used to inform clinical practice,
or referenced by the media as validated information.

Ursolic Acid-Enriched Fraction Attenuates Diabetic Cardiomyopathy Through Modulation of Inflammatory and Oxidative Stress: An Integrated in-silico and in-vivo Approach

Yashaswi Biruduraju
St. Pauls college of pharmacy
Anusha Komati
anusha.komati77@gmail.com
St. Pauls college of pharmacy
Kiranmai Mandava
St. Pauls college of pharmacy
Sneha Thakur
St. Pauls college of pharmacy
Anusha Talari
St. Pauls college of pharmacy
Deepak Rawool
ICAR - National Meat Research Institute
M Gowtham
ICAR - National Meat Research Institute

Article

Keywords: Ursolic acid-enriched fraction, Diabetic cardiomyopathy, TLR4, NF-κB, NLRP3 inflammasome, Pyroptosis, Oxidative stress, Cardioprotection

Posted Date: November 24th, 2026

DOI: https://doi.org/10.21203/rs.3.rs-11534119/v1

License: This work is licensed under a Creative Commons Attribution 4.0 International License.
Read Full License

Additional Declarations: No competing interests reported.

Ursolic Acid-Enriched Fraction Attenuates Diabetic Cardiomyopathy Through Modulation of Inflammatory and Oxidative Stress: An Integrated *in-silico* and *in-vivo* Approach

Yashaswi Biruduraju[1], Anusha Komati[2*], Kiranmai Mandava[3], Sneha Thakur[4], Anusha Talari[1], Deepak Rawool[5] Gowtham M[6]

[1]*M.Pharmacy, Department of Pharmacology, St. Pauls College of Pharmacy, Turkayamjal, Telangana, India-501510*

[2]*Associate Professor, Department of Pharmacology, St.Pauls College of Pharmacy, Turkayamjal, Telangana, India-501510, email.id:Anusha.Komati77@gmail.com; ORCID id: 0000-0002-7487-2237.3*

[3]*Professor, Department of Pharmaceutical Chemistry, St.Pauls College of Pharmacy, Turkayamjal, Telangana, India-501510,*

[4]*Professor, Department of Pharmacognosy, St.Pauls College of Pharmacy, Turkayamjal, Telangana, India-501510*

[5]*Principal Scientist, ICAR National Meat Research Institute/ ICAR-Indian Veterinary Research Institute; Hyderabad, India. email.id: deepak.rawool@yahoo.com*

[6]*ICAR-NationalMeatResearchInstitute/ICAR-Indian Veterinary Research Institute;*

Hyderabad, India. email.id: gowtham.vet1518@gmail.com

***Corresponding author**

Dr. Anusha Komati

Department of Pharmacology

St.Pauls College of Pharmacy

Telangana, India

Email: Anusha.komati77@gmail.com, anushakomati@stpaulscollege.ac.in

Phone: +91 9849640482

Abstract

Diabetic Cardiomyopathy (DCM), which is a severe complication of diabetes, has become the leading cause of heart failure in diabetic patients. Role of TLR4-NLRP3 inflammaosome signalling in the pathogenesis of DCM and effect of ursolic acid on DCM is not well explored. The present study evaluated the cardioprotective potential of ursolic acid-enriched fraction (UAEF) using a multi-targeted approach which includes in vitro, in vivo, network pharmacology, and molecular docking studies. Diabetic cardiomyopathy (DCM) was induced in male Wistar rats by streptozotocin (STZ-55mg/kg, ip) and lipopolysaccharide (LPS; 1mg/kg, ip) administration followed by treatment with UAEF at doses of 25 and 50 mg/kg and with metformin (100 mg/kg) as the reference drug. UAEF significantly inhibited α-glucosidase enzyme, free radicals (hydroxyl; $p<0.0132$, superoxide; $p<0.0241$, and nitricoxide; $p<0.0241$), and advanced glycation end-products ($p<0.0136$). UAEF contained more 59.35% ursolic acid as evidenced by quantitative RP-HPLC analysis (RT-15.5 minute). Network pharmacology identified 29 common targets, TLR4, NF-κB, TNF-α, IL-1β, RAGE, NLRP3, TXNIP, caspase-1, GSDMD, SIRT1, PGC-1α and TNNT2 emerging as major hub genes. KEGG pathway analysis further identified significant enrichment of the TLR4 signalling pathway, NF-Kb, AGE-RAGE pathway, SIRT pathway AMPK pathway and NLRP3 inflammasome-related signaling pathways. Major hub genes further validated by Molecular docking and qRT-PCR analysis and found that ursolic acid showed favorable predicted affinity for NLRP3 (−10.5 kcal/mol), IL-1β (−9.3 kcal/mol) and caspase-1 (−8.4 kcal/mol) and significant upregulation of mRNA expression of troponin TNNT2 (p<), SIRT1 ($p<0.003$), PGC-1α ($p<0.001$), TXNIP and downregulation of TLR4, NF-κB, TNF-α, IL-1β, RAGE, NLRP3, caspase-1, GSDMD ($p<0.0001$). UAEF improved post parandial glycemic load (p<), Furthermore, UAEF attenuated significantly lipid peroxidation (MDA and 4-HNE; $p <0.0001$), and protein oxidation markers (AOPP; $p <0.0001$), while significantly restoring catalase and glutathione peroxidase activities ($p <0.0001$). UAEF treatment also improved mitochondrial respiratory chain complex activities, with the 50 mg/kg dose significantly enhancing Complex I ($p < 0.0019$) Complex II ($p <0.0029$), Complex III ($p < 0.0080$), Complex IV ($p < 0.0001$), aconitase ($p < 0.0001$), and succinate dehydrogenase activities ($p < 0.0001$). Histological analysis demonstrated that UAEF significantly preserved myocardial fibrosis, reduced structural disruption, and decreased inflammatory changes. Metformin also displayed significant protection ($p<0.0001$). These results suggested that UAEF can prevent and mitigate the development of DCM and associated complications.

Keywords: Ursolic acid-enriched fraction; Diabetic cardiomyopathy; TLR4; NF-κB; NLRP3 inflammasome; Pyroptosis; Oxidative stress; Cardioprotection

1. Introduction

Diabetic cardiomyopathy (DCM) mainly refers to myocardial metabolic dysfunction caused by high glucose, and hyperglycemia is an independent risk factor for cardiac function in the absence of coronary atherosclerosis and hypertension. DCM, which is a severe complication of diabetes, has become the leading cause of heart failure in diabetic patients[1-3]. Diabetic Cardiovascular disease is the primary cause of death in diabetic patients and diabetic cardiomyopathy[5] (DCM) is characterized by hypertrophy, fibrosis, impaired ventricular function[6,7] and progressive cardiac dysfunction [4]. The involved mechanisms include oxidative stress, lipid accumulation, mitochondrial dysfunction, inflammation, cardiomyocyte apoptosis and extracellular matrix alterations [8]. Inflammatory mediators such as tumor necrosis factor-α (TNF-α), interleukin-1β (IL-1β), and IL-6 further aggravate the process of myocardial injury [9].

The gut–heart axis has been identified as a key link between metabolic dysfunction and cardiovascular inflammation. Diabetes-associated intestinal barrier dysfunction may favor LPS translocation into the circulation, thus exacerbating metabolic endotoxemia and systemic inflammation [10,11]. Gut-derived endotoxemia has been associated with inflammatory processes in the cardiovascular system [12]. LPS activates TLR4 and the subsequent inflammatory pathways [13,14,15], including NF-κB, which has been associated with DCM [16]. NF-κB-associated inflammation can favor the activation of the NLRP3 inflammasome, resulting in the activation of caspase-1, maturation of IL-1β and IL-18, and subsequent pyroptosis[18,19]. These processes have been associated with the progression of DCM [17,20].

Ursolic acid (UA) is a pentacyclic triterpenoid with reported cardioprotective, anti-inflammatory, antidiabetic and antioxidant properties [21]. Ursolic acid has been found to improve glucose and lipid metabolism [24], insulin sensitivity and inflammation [25], and have

also demonstrated metabolic, antioxidant and anti-inflammatory effects [22,23]. An ursolic acid has also been reported to reduce oxidative stress, inflammation, and fibrosis in diabetic cardiomyopathy [26]. UAEF effect on LPS-associated TLR4/NF-κB/NLRP3 signalling are, however, still incompletely understood. As a result, the present study assessed the cardioprotective effects of UAEF in an LPS-induced DCM model using integrated in vitro, in vivo, network pharmacology, and molecular docking approaches. The assessment included glycaemic control, cardiac injury, oxidative stress, mitochondrial function, inflammatory and pyroptosis-related gene expression, and cardiac histopathology.

2. Materials and Methods

2.1 Materials

Streptozotocin (STZ), nicotinamide adenine dinucleotide (NADH), cytochrome *c*, dichlorophenolindophenol (DCPIP), thiobarbituric acid (TBA), 2,4-dinitrophenylhydrazine (DNPH), 5,5′-dithiobis-(2-nitrobenzoic acid) (DTNB), epinephrine, reduced glutathione (GSH), hydrogen peroxide (H_2O_2), bovine serum albumin (BSA), methylglyoxal, sodium succinate, ethylenediaminetetraacetic acid (EDTA), sodium carbonate, sodium bicarbonate, sodium hydroxide, sodium azide, potassium ferricyanide, potassium phosphate, Tris base, mannitol, sucrose, guanidine hydrochloride, acetic acid, sodium chloride, potassium iodide, sodium citrate, hydrochloric acid, sulfuric acid, and other analytical-grade chemicals used for biochemical, oxidative stress, antioxidant, mitochondrial enzyme, and tricarboxylic acid (TCA) cycle enzyme assays were aquired from **Sisco Research Laboratories Pvt. Ltd. (SRL, Mumbai, Maharashtra, India)** and **Tokyo Chemical Industry Co., Ltd. (TCI, Tokyo, Japan)**. The **PrimeScript™ cDNA Synthesis Kit** and **TB Green® Premix Ex Taq™ II (SYBR® Green)** used for complementary DNA (cDNA) synthesis and quantitative real-time polymerase chain reaction (qRT-PCR) analyses were obtained from **Takara Bio Inc. (Shiga, Japan)**. Primary antibodies against nephrin, podocin, receptor for advanced glycation end products (RAGE), NLRP3, caspase-1, gasdermin D (GSDMD), interleukin-1β (IL-1β), and β-actin, along with horseradish peroxidase (HRP)-conjugated secondary antibodies, were obtained. Hematoxylin and eosin (H&E), periodic acid Schiff (PAS), and Masson's trichrome staining kits used for histopathological analysis were obtained. Unless otherwise specified, all other chemicals, reagents, solvents, molecular biology consumables, and laboratory-grade materials were of analytical grade and procured from authorized local vendors. Ursolic acid enriched fraction (UAEF) was obtained as gift samples from CSIR-Central Institute of Medicinal Aromatic Plants (CSIR-CIMAP), Hyderabad, Telangana, India.

2.2 Methods

2.2.1 RP-HPLC Analysis of Ursolic Acid-Enriched Fraction

Reverse-phase high-performance liquid chromatography (RP-HPLC) was employed for the chromatographic detection and validation of ursolic acid in the ursolic acid-enriched fraction (UAEF). The separation was performed via a reverse-phase ODS column. The retention duration of the ursolic acid standard was compared with the retention duration of the UAEF sample. A peak that emerges at a comparable retention time to the standard is deemed indicative of ursolic acid's existence in UAEF [27,28]. A standard solution of ursolic acid at a concentration of 60 µg/mL was formulated in an appropriate solvent. The RP-HPLC apparatus was equipped with a Phenomenex Sphereclone ODS (2) column measuring 4.6 × 250 mm with a particle size of 5 µm. Methanol and acetonitrile were employed as the solvent system in a ratio of 0.16:0.64. The flow rate was sustained at 0.4 mL/min. The ursolic acid standard solution was introduced into the HPLC apparatus, and the chromatogram was documented. The retention duration of the ursolic acid standard was ascertained. The UAEF was appropriately diluted, filtered, and introduced into the HPLC system under identical chromatographic parameters. The chromatogram acquired for UAEF was juxtaposed with that of the ursolic acid standard. The detection of a peak at a retention period aligned wit the standard (about 15.5 min) was deemed evidence of ursolic acid in UAEF.

2.2.2 Determination of λmax of Ursolic Acid

The λmax of ursolic acid was determined by a UV-Visible spectrophotometer. λmax is the wavelength at which ursolic acid shows maximum absorption. The wavelength showing maximum absorbance in UV spectrum was selected for further spectrophotometric study [29,30]. A suitable solvent was used to prepare a fine solution of ursolic acid. The UV–Visible spectrophotometer was switched on and allowed to equilibrate. The corresponding solvent served as the control. The formulated ursolic acid solution was placed into a pristine quartz cuvette. The absorption spectra of ursolic acid was obtained by scanning the relevant UV wavelength range. From the obtained spectra, the peak wavelength of absorbance was found. Ursolic acid exhibited peak absorption at around 214 nm. Hence, 214 nm was selected as λmax/analytical wavelength for ursolic acid in further spectrophotometric measurements. Ursolic acid was quantified in UAEF by using standard graph of ursolic acid

2.3. Network Pharmacology

In the present study, a comprehensive network pharmacology approach was used to investigate the possible therapeutic targets and pathways of ursolic acid (UA) in diabetic cardiomyopathy (DCM). DCM-related genes were retrieved from GeneCards, and potential UA targets were retrieved by SwissTargetPrediction and Similarity Ensemble Approach (SEA)[31-33]. The identified targets were mapped to official Homo sapiens gene nomenclature, and duplicate entries were removed. A total of 105 targets associated with UA and 512 genes related to DCM were identified, and Venn analysis revealed 29 common targets, which are possible therapeutic targets of UA in DCM. The common targets were analyzed by STRING protein-protein interaction analysis and visualized by Cytoscape, and topological features were used to identify potential hub genes [34,35]. DAVID enrichment analysis suggested roles in inflammatory responses, oxidative stress, fatty acid metabolism, transcriptional regulation, and cardiac structural functions [36]. KEGG pathway enrichment analysis suggested roles in TLR, NF-κB, NOD-like receptor/NLRP3, AGE-RAGE, PI3K-Akt, AMPK, MAPK, apoptosis, and metabolic pathways[37-39]. Considering the essential function of the TLR4/NF-κB/NLRP3 pathway in inflammation and cardiomyocyte injury in DCM, we paid particular attention to it. Then, a UA-target-pathway network was constructed by Cytoscape, and UA may exert cardioprotective effects through the coordination of the regulation of inflammation, oxidative stress, lipid and energy metabolism, and cardiomyocyte injury [40]. The network pharmacology analysis identified 29 potential shared targets, providing a systems-level basis for investigating the molecular mechanisms of UA in DCM and supporting further experimental validation.

2.4. Molecular Docking

Molecular docking analysis was performed to investigate the potential binding interactions of ursolic acid with selected protein targets associated with diabetic cardiomyopathy and the TLR4/NF-κB/NLRP3 inflammatory signalling pathway. The selected target proteins included Caspase-1, NLRP3, TLR4, TNF-α, IL-1β and TNNT-2, for which the corresponding three-dimensional protein structures were obtained based on their respective Protein Data Bank (PDB) identifiers. Ursolic acid was used as the ligand, and molecular docking was performed using PyRx with AutoDock Vina to estimate the binding affinity of the ligand towards the selected target proteins [41,42]. The predicted binding affinities were expressed in kcal/mol, with more negative values indicating relatively stronger predicted binding. The docked complexes were subsequently visualized using three-dimensional and docking interaction representations to examine the possible ligand–protein interactions. The docking results were

used to provide additional computational support for the potential involvement of these targets in the cardioprotective mechanism of the ursolic acid-enriched fraction.

2.5. *In vitro* studies

2.5.1. *In vitro* antioxidant and anti-glycation activities of Ursolic acid-enriched fraction

The antioxidant potential of the ursolic acid-enriched fraction was evaluated by determining its hydroxyl radical, superoxide radical, and nitric oxide radical scavenging activities, along with its inhibitory effect on advanced glycation end-product (AGE) formation using established in vitro methods [47–50]. Hydroxyl radical scavenging activity was determined using the deoxyribose degradation assay with slight modifications [47]. Briefly, 20 µL of Ursolic acid-enriched fraction solution (5 mg/mL prepared in DMSO) was mixed with 100 µL of 2-deoxy-D-ribose (2.8 mM), $FeCl_3$ (0.1 mM), EDTA (0.1 mM), H_2O_2 (10 mM), ascorbic acid (0.1 mM), and 400 µL of KH_2PO_4–KOH buffer (20 mM, pH 7.4), followed by incubation at 37°C for 1 h. The reaction was terminated by adding 1 mL of 1% thiobarbituric acid (TBA), heated at 95°C for 20 min, and the absorbance was measured at 532 nm using a UV–visible spectrophotometer. Hydroxyl radical scavenging activity was expressed as the percentage inhibition of thiobarbituric acid-reactive substance formation. Superoxide radical scavenging activity was assessed using the riboflavin–nitro blue tetrazolium (NBT) photoreduction method [48]. The reaction mixture comprised 20 µL of Ursolic acid-enriched fraction (5 mg/mL in DMSO), 0.2 mL EDTA, 0.1 mL NBT, 0.05 mL riboflavin, and 2.64 mL phosphate buffer (0.1 M, pH 7.2), whereas DMSO served as the control. After incubation for 30 min, the absorbance was recorded at 560 nm, with gallic acid used as the positive control.

Superoxide radical scavenging activity was calculated as the percentage inhibition of superoxide generation. Nitric oxide scavenging activity was determined using sodium nitroprusside as the nitric oxide donor [49]. The reaction mixture containing 200 µL sodium nitroprusside, 50 µL phosphate-buffered saline (PBS, pH 7.4), and 50 µL Ursolic acid-enriched fraction solution (5 mg/mL in DMSO) was incubated at 25°C for 30 min, followed by the addition of 50 µL of Griess reagent and further incubation for 30 min. The absorbance was measured at 546 nm, and nitric oxide scavenging activity was expressed as the percentage inhibition relative to the control. The anti-glycation potential of the ursolic acid-enriched fraction was evaluated using an in vitro bovine serum albumin (BSA)-methylglyoxal glycation model [50]. BSA (10 mg/mL) was incubated with 1 mM methylglyoxal in phosphate-buffered saline (100 mM, pH 7.4) containing 0.02% sodium azide in the presence or absence of Ursolic acid-enriched fraction (5 mg/mL), while aminoguanidine (5 mg/mL) served as the reference

anti-glycation agent. BSA incubated without methylglyoxal was used as the blank. The reaction mixtures were maintained at 37°C for 1, 3, and 7 days, and AGE formation was quantified by measuring fluorescence intensity at an excitation wavelength of 355 nm and an emission wavelength of 460 nm. The anti-glycation activity of the ursolic acid-enriched fraction was expressed as the percentage inhibition of fluorescent AGE formation compared with the glycated control.

2.6 RNA Extraction and Quantitative Real-Time Polymerase Chain Reaction (qRT-PCR)

Cardiac tissues were collected from streptozotocin (STZ; 55 mg/kg)-induced diabetic rats treated with or without Ursolic acid-enriched fraction (UAEF;25and 50mg/kg) for 21 days. At the end of the experimental period, cardiac tissues were harvested, immediately processed, and used for total RNA isolation. Total RNA was extracted using TRIzol® reagent (Life Technologies, USA) according to the manufacturer's instructions [43]. The STZ induction protocol and UAEF treatment doses were selected based on previously published studies demonstrating the reliable induction of diabetic cardiomyopathy and the cardioprotective effects of UAEF in experimental models [44].

The concentration and purity of the isolated RNA were determined spectrophotometrically using a BioSpec-nano spectrophotometer (Shimadzu, Kyoto, Japan). RNA samples with appropriate purity were subsequently used for complementary DNA (cDNA) synthesis. Equal amounts of total RNA were reverse-transcribed into cDNA using the PrimeScript™ cDNA Synthesis Kit (Takara Bio Inc., Shiga, Japan) according to the manufacturer's protocol.Gene-specific primers were designed using the NCBI Primer-BLAST database and Primer3 software (version 0.4.0) [45,46]. The expression levels of genes associated with inflammation, oxidative stress, pyroptosis, inflammasome activation, and diabetic cardiomyopathy, and the expression of genes involved in diabetic cardiomyopathy-associated inflammatory, oxidative stress, pyroptotic, mitochondrial, and cardiac structural signaling, including *Casp1, Sirt1, Gsdmd, Tnf, Ppargc1a, Il1b, Txnip, Nfkb1, rage, Nlrp3, Tnnt2,* and *Tlr4*, were evaluated. The sequences of the forward and reverse primers used for quantitative real-time PCR (qRT-PCR) are presented in Table 1. Quantitative real-time PCR (qRT-PCR) was performed using TB Green® Premix Ex Taq™ II (Takara Bio Inc., Shiga, Japan) according to the manufacturer's instructions. β-actin (Actb) was used as the endogenous housekeeping gene for normalization of gene expression. The relative expression levels of the target genes were calculated using the comparative threshold cycle ($2^{-}\Delta\Delta Ct$) method. The results were expressed as fold changes relative to the respective control group.

Table 1. Primer sequences used for gene expression analysis by quantitative real-time polymerase chain reaction (qRT-PCR).

S.NO	PRIMERS	FORWARD (5'-3')	REVERSE (3'-5')
1	Caspase-1	ACTCGTACACGTCTTGCCCTCA	CTGGGCAGGCAGCAAATTC
2	SIRT-1	TGCTGGCCTAATAGAGTGGCA	CTCAGCGCCATGGAAAATGT
3	Gasdermin D	AAGATCGTGGATCATGCGT	AAGATCGTGGATCATGCCGT
4	TNF-α	AAGGTCAACCTCCTCTCT	CAGATAGATGGGCTCATACC
5	IL-1β	GAATTTGAGTCTGCCCAGTT	CCATGCTGAAGTCAATTAGGT
6	TXNIP	GTGATAGTGGAGGTGTGTGAAG	CAGGTACTCCGAAGTCTGTTTG
7	NFκB	GGCTCAACATCTACACAGT	GTCCTTGCGGAAGTCAAT
8	β-Actin	CAGGTCATCACCATTGGCAATGAGC	CGGATGTCCACGTCACACTTCATGA
9	TNNT2	GAG AAG AAG GAG GAG GAGGA	TCT TGG TCT TGG TCT TGG TT
10	RAGE	GTGTCCTTCCCAACGGCTC	ATTGCCTGGCACCGGAAAA
11	TLR-4	AGATTGCTCAGACCTGGCAG	CACTGAGTCCAGAGGGAATG
12	NLRP-3	TGTCGGGAGGTGAGCCTTGTG	GATCTTGTGGATGGGTGGGTTTGG

2.7 In vivo studies

2.7.1 Experimental animals and ethical approval

Healthy adult male Wistar albino rats (8–10 weeks old) weighing between 200 and 250 g were obtained from the institutional animal facility and used for the present investigation. Animals were housed under standard laboratory conditions at a temperature of 22 ± 2°C, relative humidity of 50–60%, and a 12 h light/dark cycle with unrestricted access to standard pellet diet and drinking water. Before the initiation of the experiment, animals were acclimatized for seven days to minimize environmental stress and physiological variations. All experimental

procedures were conducted in accordance with the guidelines of the Committee for the Purpose of Control and Supervision of Experiments on Animals (CPCSEA) [51], Government of India, and the study protocol was approved by the Institutional Animal Ethics Committee (IAEC) of St. Pauls College of Pharmacy, Turkayamjal, Hyderabad-501510, Telangana, India. Approval Number is **SPCP/2025-2026/COL/01**. Animal care and handling were performed following internationally accepted guidelines for laboratory animal research.

2.7.2 Induction of experimental diabetes

Following a 7-day acclimatization period, baseline body weight, fasting blood glucose (FBG), and an oral glucose tolerance test (OGTT) were recorded. Experimental diabetes was induced by repeated intraperitoneal administration of streptozotocin (STZ) at a cumulative dose of 55 mg/kg body weight[52], administered in four divided doses on Days 1, 4, 6, and 10. STZ was freshly dissolved in ice-cold 10 mM citrate buffer (pH 4.5) immediately before each injection. Control animals received an equivalent volume of citrate buffer. Following each STZ administration, rats were provided with 5% glucose solution for 24 h to prevent acute hypoglycemia. Fasting blood glucose levels were monitored throughout the induction period using a glucometer. Animals with fasting blood glucose levels ≥250 mg/dL after the final STZ administration were considered diabetic and included in the study. After induction of diabetes, lipopolysaccharide (LPS) at 1mg/kg was administered intraperitoneally to mimic inflammatory conditions.

2.7.3 Experimental grouping and treatment protocol

After confirmation of diabetes, animals were randomly divided into five experimental groups consisting of six rats in each group. Group I served as the normal control and received vehicle treatment throughout the study. Group II served as the diabetic cardiomyopathy control and received STZ along with LPS administration. Group III comprised diabetic rats treated with low-dose Ursolic acid-enriched fraction[25mg/kg], whereas Group IV consisted of diabetic rats receiving high-dose Ursolic acid-enriched fraction[50mg/kg]. Group V served as the standard treatment group and received Metformin[100mg/kg], a clinically established antidiabetic agent. Ursolic acid-enriched fraction and Metformin were administered orally once daily for four weeks. Vehicle-treated groups received equivalent volumes of the dosing vehicle. Throughout the treatment period, animals were observed daily for general health status, food intake, water consumption, and any evidence of drug-related toxicity.

2.7.4 Monitoring of physiological and cardiac function parameters

Weekly assessment of body weight and blood glucose (BG) was done throughout the duration of the experiment to monitor the progress of developing diabetes and the effect of the ursolic acid-enriched fraction as treatment. Weight measurement was performed using the digital weighing scale while BG measurement was done using the glucometer after overnight fasting [53].

2.7.5 Tissue sample collection

At the end of the experimental period, the animals were anaesthetized using Ketamine (80mg/Kg, Intraperitoneally) and xylazine (10mg/kg, Intraperitoneally) and cervical dislocation was performed under anaesthesia, and the animals were sacrificed according to the approved institutional animal ethical guidelines. the hearts were immediately isolated, rinsed thoroughly with ice-cold normal saline to remove residual blood, blotted dry, and weighed. The heart tissue was carefully dissected and homogenized in ice-cold phosphate-buffered saline (PBS; pH 7.4) or an appropriate homogenization buffer. The tissue homogenates were centrifuged at 10,000 × g for 15 min at 4°C, and the resulting supernatants were collected and stored at −80°C until further biochemical, oxidative stress, inflammatory, mitochondrial, and molecular analyses. cardiac tissues were fixed in 10% neutral-buffered formalin for histopathological study.

Lipid Peroxidation assays

Cardiac oxidative stress, antioxidant defence status, mitochondrial electron transport chain (ETC) enzyme activities, and tricarboxylic acid (TCA) cycle enzyme activities were evaluated in left ventricular tissue homogenates using established spectrophotometric methods. Lipid peroxidation was assessed by estimating malondialdehyde (MDA) levels as Thiobarbituric acid-reactive substances (TBARS). Briefly, cardiac tissue homogenates were incubated with thiobarbituric acid reagent under acidic conditions, heated in a boiling water bath, cooled, and centrifuged. The absorbance of the resulting chromogen was measured at 532 nm, and MDA levels were expressed as an index of lipid peroxidation and oxidative damage [54].

Antioxidant assays

Superoxide dismutase (SOD) activity was determined based on its ability to inhibit the auto-oxidation of epinephrine in carbonate buffer (pH 10.2), and the change in absorbance was recorded at 480 nm [55]. Catalase (CAT) activity was measured by monitoring the decomposition of hydrogen peroxide at 240 nm [56]. Reduced glutathione (GSH) content was estimated using 5,5′-dithiobis-(2-nitrobenzoic acid) (DTNB; Ellman's reagent), and the

absorbance of the resulting yellow-colored chromogen was measured at 412 nm [57]. Glutathione peroxidase (GPx) activity was determined according to the standard enzymatic method based on the oxidation of reduced glutathione in the presence of hydrogen peroxide [58].

Protein oxidation assays

Protein oxidation was assessed by estimating advanced oxidation protein products (AOPP) using chloramine-T as the standard, whereas protein thiol (–SH) content was determined using DTNB reagent, and absorbance was measured at 412 nm [59]. These parameters were used to evaluate oxidative stress and the antioxidant potential of the ursolic acid–enriched fraction in streptozotocin- and lipopolysaccharide-induced diabetic cardiomyopathy.

Mitochondrial Complexes and TCA enzymes

Mitochondrial function was evaluated by determining the activities of electron transport chain (ETC) complexes I–IV in cardiac tissue homogenates. Complex I (NADH: coenzyme Q oxidoreductase) activity was determined by monitoring the oxidation of NADH in the presence of coenzyme Q at 340 nm. Complex II (succinate: coenzyme Q oxidoreductase) activity was measured using sodium succinate as the substrate and dichlorophenolindophenol (DCPIP) as the electron acceptor, with absorbance monitored at 600 nm. Complex III (coenzyme Q: cytochrome c oxidoreductase) activity was assessed by measuring the reduction of oxidized cytochrome c at 550 nm, whereas Complex IV (cytochrome c oxidase) activity was determined by monitoring the oxidation of reduced cytochrome c at the same wavelength. The activities of ETC complexes were normalized to total protein content and expressed as units per milligram of protein [60].

The activities of key tricarboxylic acid (TCA) cycle enzymes, including succinate dehydrogenase (SDH) and aconitase, were also determined spectrophotometrically using established methods. SDH activity was estimated based on the reduction of potassium ferricyanide in the presence of sodium succinate as the substrate [61], whereas aconitase activity was measured using citrate as the substrate by monitoring the formation of reaction products spectrophotometrically [62]. All biochemical analyses were performed in triplicate using validated protocols. Total protein concentration in cardiac tissue homogenates was determined by the Bradford method, and enzyme activities were normalized to protein content and expressed as units per milligram of protein [63]. Collectively, these biochemical parameters were used to evaluate mitochondrial function, oxidative stress, and the

cardioprotective efficacy of the ursolic acid enriched fraction in experimental diabetic cardiomyopathy.

2.7.7 Histopathological studies

Cardiac tissues were immediately fixed in 10% neutral-buffered formalin, processed using the conventional paraffin-embedding technique, and sectioned into 4–5 μm thick slices using a rotary microtome. The tissue sections were subsequently stained with hematoxylin and eosin (H&E) for the assessment of general myocardial architecture, Masson's trichrome for the evaluation of collagen deposition and myocardial fibrosis, following standard histopathological procedures.

Histopathological evaluation was performed using a light microscope at 20× and 40× magnifications by an observer blinded to the treatment groups. Representative photomicrographs were captured to assess myocardial structural integrity, including cardiomyocyte arrangement, myocardial fiber disorganization, cellular degeneration, inflammatory cell infiltration, interstitial edema, vascular congestion, myofibrillar disruption, collagen deposition, and fibrosis associated with streptozotocin- and lipopolysaccharide-induced diabetic cardiomyopathy. Histopathological findings were qualitatively compared among the experimental groups to determine the cardioprotective effects of the ursolic acid-enriched fraction against diabetes-induced myocardial injury and adverse cardiac remodeling [64–66]. The interstitial collagen formation was calculated using Image J Software and percentage was calculated using following formula Collage area/ Total area x 100.

2.7.8 Statistical analysis

All experimental data were expressed as mean ± standard error of the mean (SEM). Statistical analyses were performed using GraphPad Prism version 8.02 (GraphPad Software Inc., San Diego, CA, USA). Data normality was assessed before statistical analysis. Comparisons between two experimental groups were performed using an unpaired two-tailed Student's *t*-test with Welch's correction. In contrast, comparisons among multiple groups were analyzed using one-way analysis of variance (ANOVA) followed by Tukey's multiple comparison post hoc test. Differences were considered statistically significant at a p-value of < 0.05.

3. RESULTS

3.1 RP-HPLC Analysis of Ursolic Acid-Enriched Fraction

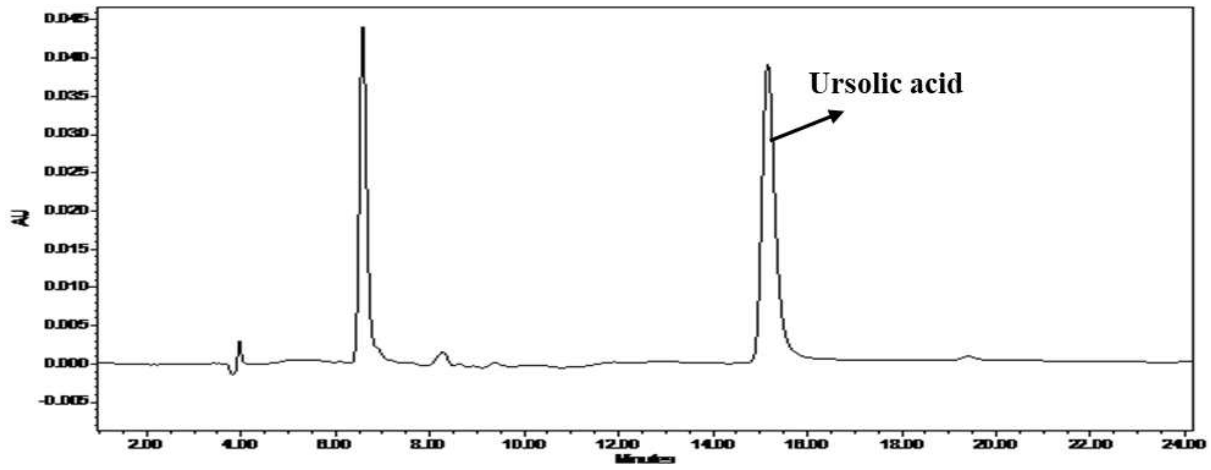


Figure3.1: RP-HPLC chromatogram of Ursolic acid Standard (60 µg/ml)

Conditions: Phenomenex Sphereclone ODS (2) column (4.6 X 250 mm, 5 µm) and Methanol and Acetonitrile (0.16:0.64) solvent system at 0.4 mL/ min.

Confirmation of ursolic acid in Ursolic Acid Enriched Fraction (UAEF) by RP-HPLC analysis. RP-HPLC analysis was performed on Phenomenex Sphereclone ODS (2) column (4.6 × 250 mm, 5 m) by using methanol and acetonitrile solvent system (0.16:0.64) at flow rate of 0.4 ml/min. Standard of ursolic acid (60 g/mL) showed a well-defined peak with retention time of around 15.5 minutes. The UAEF showed a peak with similar retention time which confirms the presence of ursolic acid in enriched fraction. The characteristic well defined peak confirms the effective chromatographic separation of ursolic acid from other constituents in UAEF. RP-HPLC analysis confirmed the presence and chromatographic characterization of ursolic acid in UAEF under chromatographic conditions adopted.

3.2 Determination of λmax of Ursolic acid

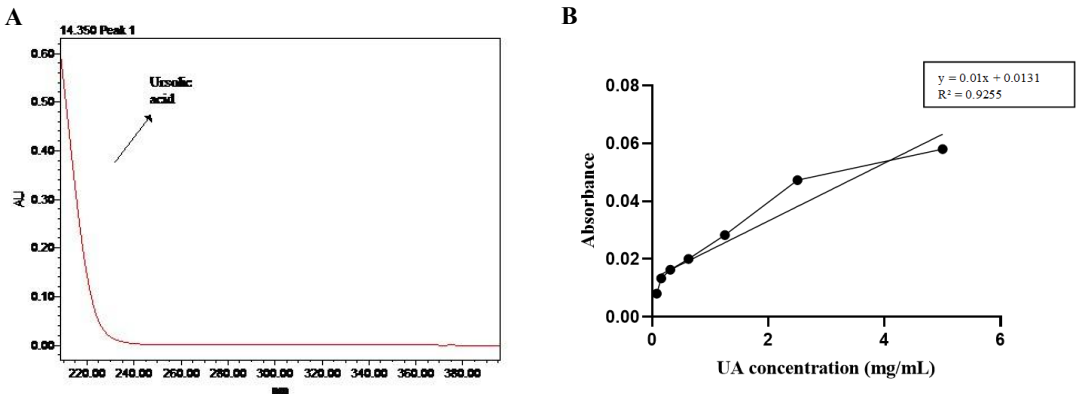


Figure 3.2. Determination of λmax of Ursolic acid quantification

A) Ursolic acid λmax was determined using UV-Visible spectroscopy and B) UA content in UAEF was quantified using a ursolic acid standard calibration curve. The UAEF showed a ursolic acid content of 59.35% (w/w), confirming substantial enrichment of ursolic acid in the fraction.

The UV–Visible spectrum of Ursolic acid was taken to find its maximum wavelength of absorption. Ursolic acid showed maximum absorption at approximately 214 nm, representing its characteristic absorption wavelength. Quantitative estimation of ursolic acid (UA) in the ursolic acid enriched fraction (UAEF) was done by using the ursolic acid standard calibration curve. ursolic acid content was found of 59.34±0.04% w/w in the fraction. The results indicated that ursolic acid was significantly enriched in UAEF, suggesting that the bioactive triterpenoid was successfully enriched during the fractionation.

3.3 Network Pharmacological analysis of ursolic acid against DCM

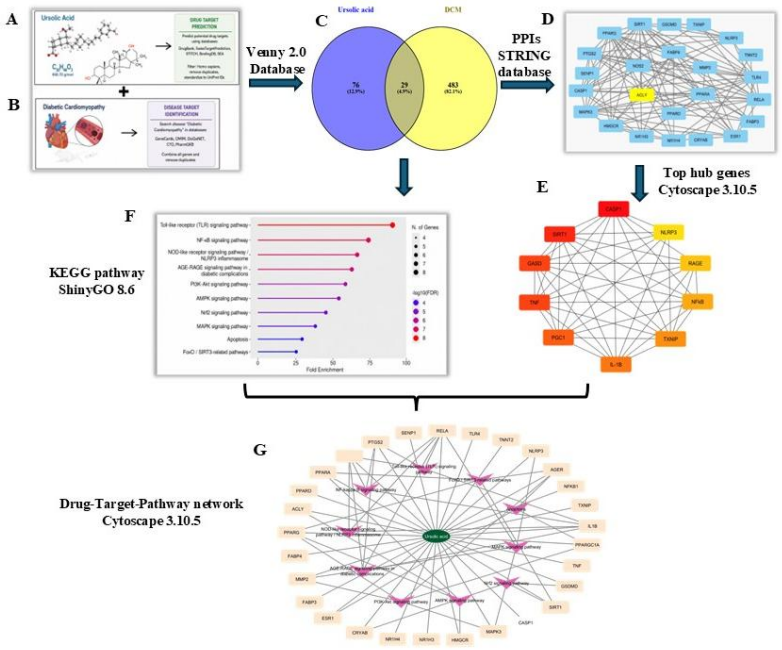


Figure 3.3. Network pharmacology for identifying the therapeutic targets and molecular pathways of Ursolic acid against Diabetic cardiomyopathy.

The schematic illustrates the comprehensive network pharmacology strategy employed to investigate the therapeutic potential of the ursolic acid against diabetic cardiomyopathy. **(A)** Identification of DCM-related targets from multiple databases, including DrugBank, Swiss Target Prediction, STITCH, Binding DB, and SEA (Similarity Ensemble Approach), followed by integration and removal of duplicate targets. **(B)** Retrieval of Diabetic cardiomyopathy-associated genes from GeneCards, DisGeNET, and MalaCards databases. **(C)** Identification of common targets by Venn diagram analysis, representing the overlap between Diabetic cardiomyopathy-associated targets and diabetic cardiomyopathy-related genes. **(D)** Construction of a protein–protein interaction (PPI) network for the overlapping targets using the STRING database. **(E)** Topological analysis of the PPI network in Cytoscape 3.10.5 to identify hub genes based on network centrality parameters. **(F)** KEGG pathway enrichment analysis of the common targets, illustrating significantly enriched biological processes using ShinyGo 8.6 database. (G) Ursolic acid-Targets-Pathway network constructed by Cytoscape 3.10.5.

To explore the potential molecular targets and signalling pathways associated with the ursolic acid against DCM, an integrated network pharmacology approach was employed (Figure 3.3). ursolic acid-associated targets were retrieved from DrugBank, SwissTargetPrediction, STITCH, BindingDB, SEA, and the Therapeutic Target Database, whereas DCM-related genes were collected from GeneCards, OMIM, PharmGKB, DisGeNET, MalaCards, Comparative Toxicogenomics Database (CTD), and TTD (Figure 3.3 A, B). After removing duplicate entries and standardizing gene symbols using UniProt, 483 DCM-associated genes and 76 UREF-

associated targets were obtained. Intersection analysis identified 29 overlapping targets, representing putative therapeutic targets for subsequent experimental evaluation (Figure3.3).

To further examine the predicted functional relationships among these overlapping targets, a protein–protein interaction (PPI) network was constructed using the STRING database. The resulting network consisted of 29nodes and 98 edges, with a highly significant PPI enrichment ($p < 1.0 \times 10^{-11}$), indicating strong biological connectivity among the identified targets (Figure 3.3D). Topological analysis of the PPI network using Cytoscape prioritized TNF, SOD2, NF-κB, IL1β, and CASP1 as top candidate hub genes based on degree, betweenness, and closeness centrality analyses, suggesting their potential involvement in oxidative stress, inflammatory signalling, apoptosis, and metabolic dysregulation associated with DCM (Figure 3.3E).

Functional enrichment analysis using ShinyGo 8.6 database predicted that the overlapping targets were significantly enriched in biological processes associated with oxidative stress response, inflammatory signalling, lipid metabolism, transcriptional regulation, and antioxidant defence. KEGG pathway enrichment analysis identified significant enrichment of pathways including pyroptosis, NLRP3 inflammasome signalling, TNF, IL-1β, NF-κB, PI3K–Akt, MAPK, HIF-1, AGE–RAGE signalling, cytokine–cytokine receptor interaction, glutathione metabolism, insulin resistance, and reactive oxygen species-related pathways, indicating potential biological pathways associated with the predicted targets (Figure 3.3F). A drug-target-pathway interaction network was subsequently constructed in Cytoscape to visualize the predicted relationships among ursolic acid, the overlapping target genes, and the significantly enriched pathways (Figure 3.3 G). These network pharmacology findings provided a systems-level framework for generating hypotheses regarding the potential molecular mechanisms of ursolic acid, which were subsequently validated through molecular docking and qRT-PCR analysis of selected target genes (Figure 3.3).

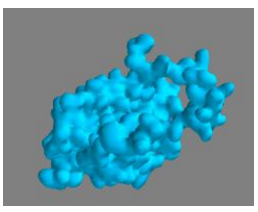
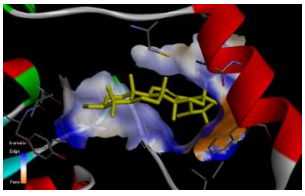
3.4 Molecular Docking analysis of ursolic acid

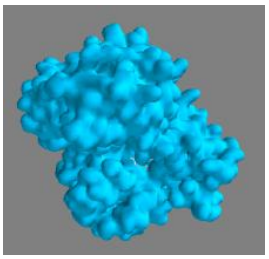
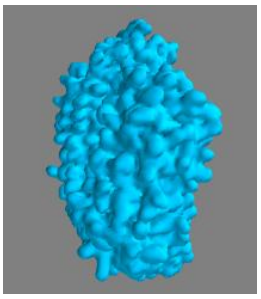
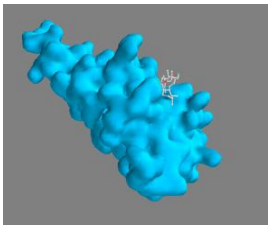
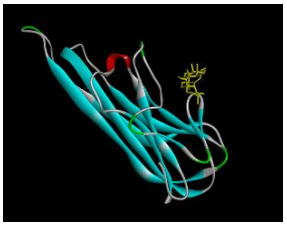
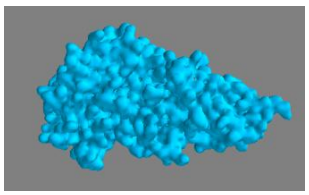
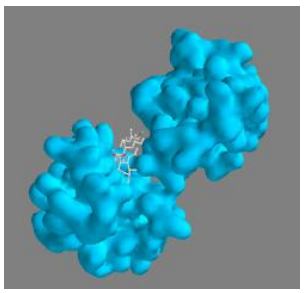
Molecular docking analysis was performed to validate binding potential of Ursolic acid against selected target proteins involved in inflammation, pyroptosis and diabetic complications (Table 3.2). The docking results revealed different binding affinities of Ursolic acid toward the selected target proteins. The selected targets with the highest predicted binding affinity were NLRP3 (−10.5 kcal/mol), IL-1β (−9.3 kcal/mol) and Caspase-1 (−8.4 kcal/mol). Ursolic acid also showed a good predicted binding affinity with TLR4 (−7.4 kcal/mol), TNNT2 (−7.0 kcal/mol) and TNF-α (−6.5 kcal/mol) (Table 3.1), these targets further validated by qRT-PCR analysis.

Table 3.1. Molecular docking analysis of Ursolic acid against selected target proteins.

S.no	Target protein	PDB ID	Binding affinity(kcal/mol)
1	Caspase-1	1RWN	-8.4
2	NLRP3	7ALV	-10.5
3	TLR4	3FXI	-7.4
4	TNF-α	1TNF	-6.5
5	IL-β	1I1B	-9.3
6	TNNT-2	4Y99	-7

Table 3.2. Three-dimensional structures and molecular docking complexes of Ursolic acid with selected target proteins.

S.NO	**Target protein**	**3D structure of target protein**	**Ursolic acid–target protein docked complex**
1	Caspase-1		

2	NLRP3		
3	TLR4		
4	TNF-α		
5	IL-1β		
6	TNNT2		

3.5 UAEF displayed antioxidant, antihyperglycemic and anti-glycation activities

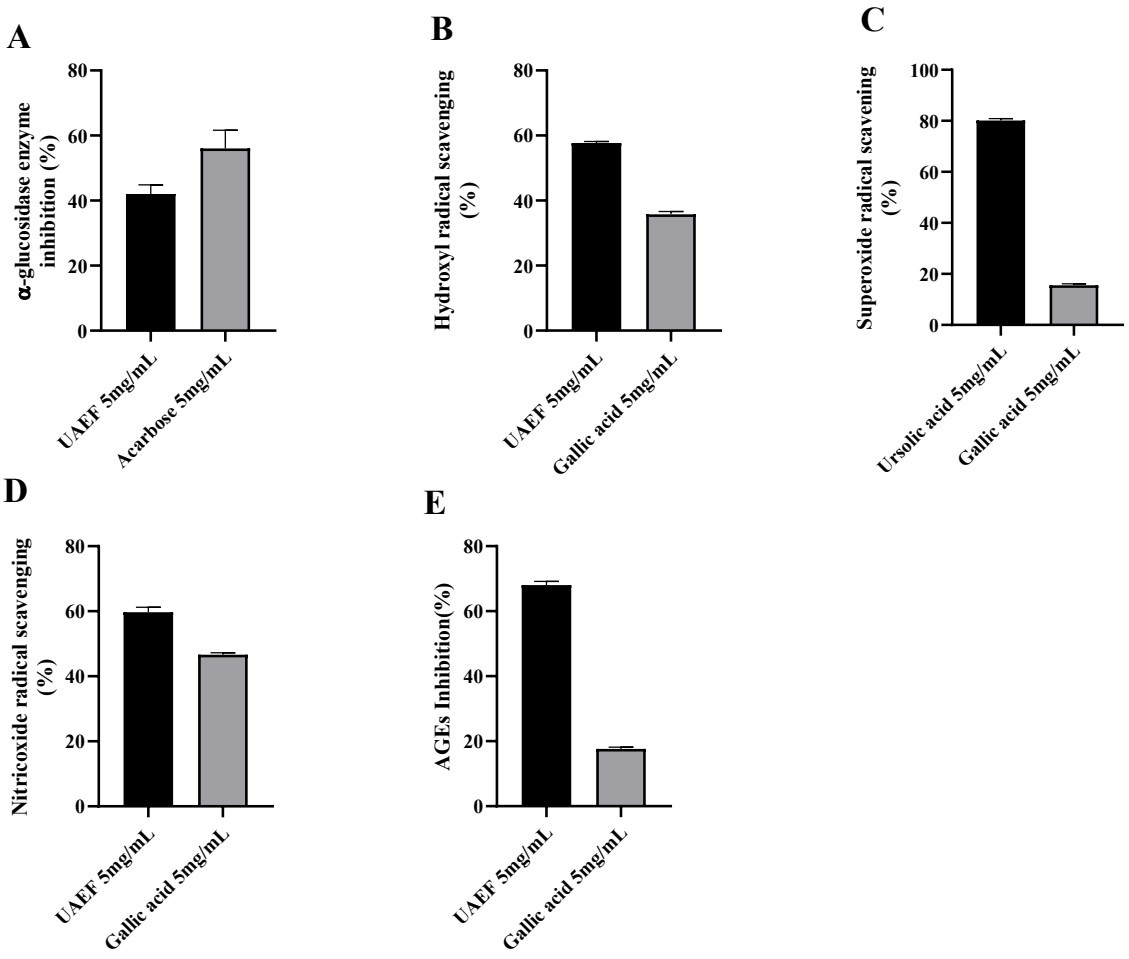


Figure3.4: UAEF effect on free radicals, alpha-glucosidase and AGEs

A) Alpha-glucosidase and free radicals scavenging (B) hydroxyl, C) superoxide, D) nitric oxide radicals and E) AGEs were incubated with UAEF (5mg/mL) and absorbances were recorded using UV-visible Spectrophotometer. Values were calculated using unpaired t-test with welch's correction and expressed as mean ± SD. All experiments were performed in triplicate (n=3).

Free radicals scavenging, alpha-glucosidase, and advanced glycation end products inhibition were measured under UAEF treatment. Figure 3.4 illustrated that UAEF 5mg/mL inhibited digestion of substrate by 26.66% (Figure3.4A). Acarbose, the standard α-glucosidase inhibitor, reduced enzyme activity by 34.6% (Figure3.4A). The hydroxyl, superoxide and nitric oxide radical scavenging potentials of UAEF are presented in Figure3.4. UAEF 5mg/mL scavenged hydroxyl radicals ($p<0.0132$), superoxide ($p<0.0241$) and nitric oxide ($p<0.0241$). Gallic acid was used as a standard. UAEF 5mg/mL significantly inhibited advanced glycation end products (AGEs) ($p<0.0\ 136$). Aminoguanidine has displayed comparable effect.

3.6 Ursolic acid-enriched fraction attenuated postprandial glycemic load in STZ-induced Diabetic cardiomyopathy (DCM) rats

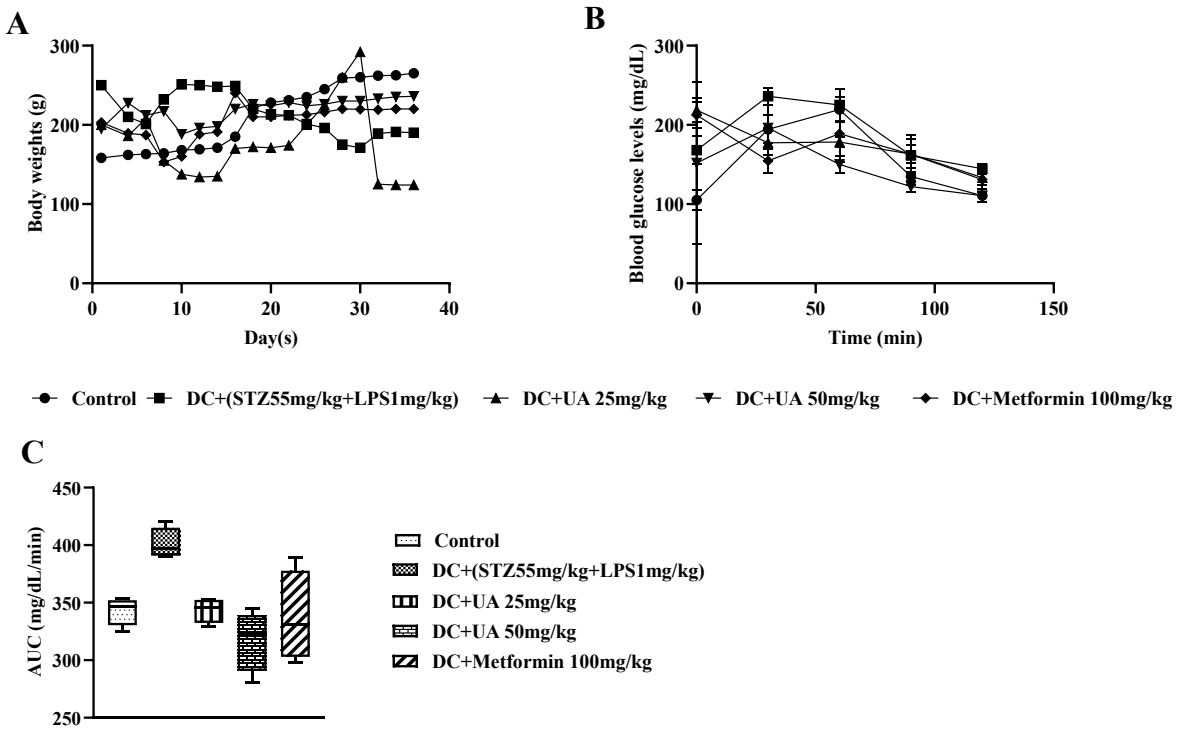


Figure 3.5: Effect of UAEF on body weight and glycemic load in DC rats.

DC rats were treated with different doses UAEF 25mg/Kg and 50 mg/Kg. A) Body weights were measured every alternative day, B) OGTT on fourth day of study, C) representative AUC of glucose levels. Results were analysed using XY analysis and one-way ANOVA, Tukey's multiple comparison post test. Values were expressed as mean±SEM, n=6. Whereas, $^{****}p<0.0001$, $^{***}p<0.001$, *vs* control and $^{####}p<0.0001$, $^{###}p<0.001$, $^{##}p<0.001$, $^{#}p<0.025$ *vs* DC.

Body weight changes following STZ (55mg/Kg) and LPS (1mg/Kg) induction and UAEF treatment in rats were measured every alternative day. Figure 3.6A illustrated that control group animals displayed a progressive increase in body weight during the experimental duration. On the other hand, the DCM group exhibited impaired weight gain compared to the control group. Body weights were significantly regained by treatment with UAEF (25 and 50 mg/Kg) and metformin (100mg/Kg); high dose of UAEF 50 mg/Kg group displayed significant ($p<0.0027$) improvement than lower dose.

The results of oral sucrose tolerance and effect of UAEF was presented in Figure 3.6B. It was found that treatment with different doses (25 and 50 mg/Kg) orally followed by glucose (2g/Kg) administration significantly reduced postprandial glycemic excursion at 0^{th} ($p<0.0001$), 30^{th} ($p<0.0008$), 60^{th} ($p<0.0197$), and 90^{th} ($p<0.0001$) min (Figure 3.6B). We took UAEF (25 and 50 mg/Kg) as treatment and metformin (100mg/Kg) as the standard for

comparison of our results. Significant inhibition in glycemic excursion was observed with UAEF treatment at 30thmin following glucose administration ($p<0.0001$) due to its inhibitory action of alpha-glucosidase enzyme (Figure 3.6A),.

The 2 h glycemic load was calculated as area under the curve (AUC). AUC was significantly enhanced in DC group compared with control group, Whereas, UAEF significantly restored AUC, specifically at 50mg/Kg representing glucose utilization (Figure 3.6D) ($p<0.0001$). Metformin treatment also reduced AUC substantially ($p<0.0001$).

3.4. UAEF attenuated oxidative stress, protein oxidation and lipid peroxidation in DCM rats

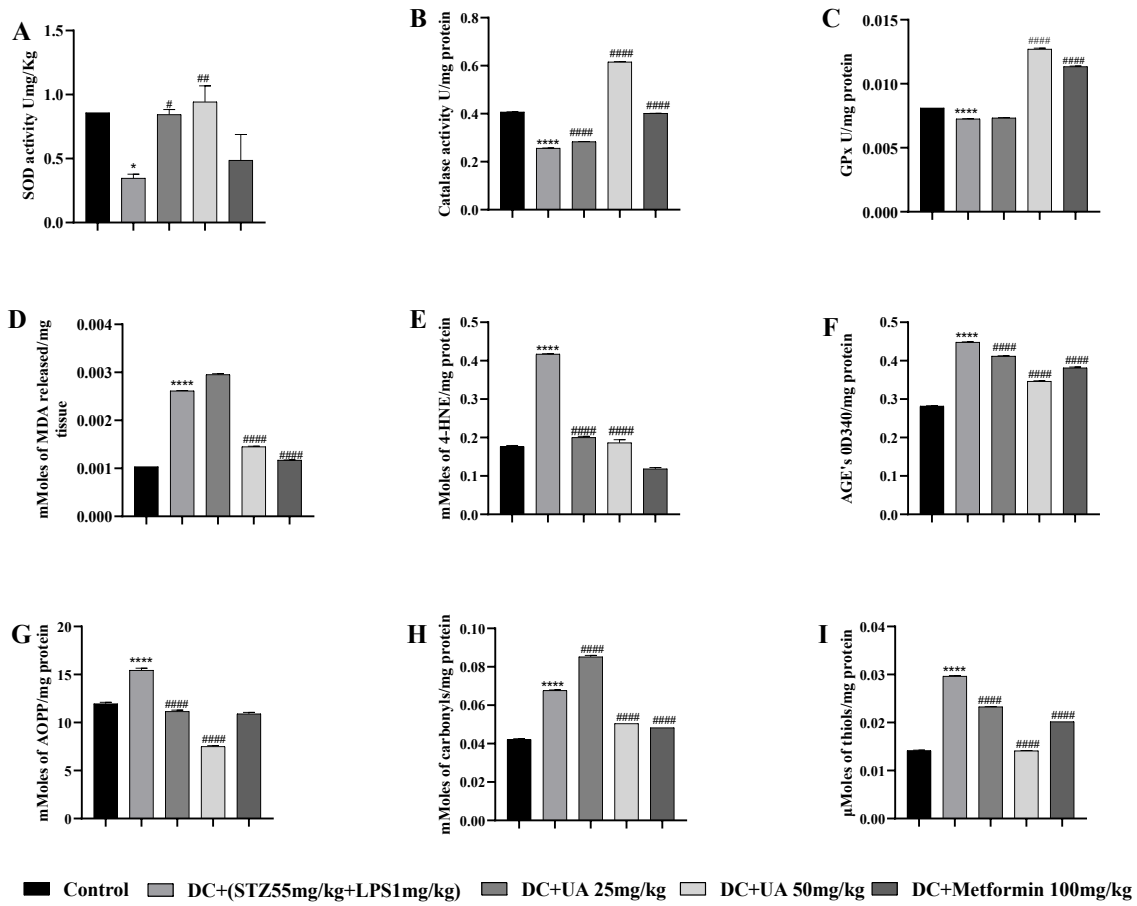


Figure 3.6: Effect of UAEF on antioxidative enzymes, protein oxidation and lipid peroxidation in DCM rats.

DC rats were treated with different doses UAEF 25mg/Kg and 50 mg/Kg. After treatment period A) SOD, B) catalase, C) Glutathione peroxidase (GPx) enzymes levels, D) MDA, E) 4-HNE, F)AGEs, G)AOPP, I) protein thiol content, H) protein carbonyl contents were measured in pooled heart homogenate using UV-Visible spectroscopic methods. Results were analyzed

using one-way ANOVA, Tukey's multiple comparison post test. Values were expressed as mean±SEM, n=6. Whereas, $^{****}p<0.0001$ *vs* control and $^{####}p<0.0001$, $^{##}p<0.0011$ *vs* DC.

STZ and LPS treatment significantly damaged cardiac tissue through the inflammation and oxidative stress, characterized by attenuated antioxidative enzymes like Superoxide dismutase (SOD), catalase, and glutathione peroxidase (GPx), proteins oxidation and lipids oxidation. Figure3.6 demonstrated that SOD, catalase and GPx levels were significantly reduced ($p<0.0001$) in DC group when compared to control group. Treatment with UAEF significantly elevated catalase (UAEF 25mg/Kg, $p<0.0001$ and 50mg/Kg, $p<0.0001$) (Figure3.6B) and GPx (UAEF 50mg/Kg, $p<0.0001$) (Figure 5.9C) levels compared with DC group. SOD levels were significantly restored with treatment (UAEF 25mg/Kg, $p<0.0001$ and 50mg/Kg, $p<0.0001$) (Figure3.6A). Metformin displayed substantial improvement in SOD ($p<0.001$), catalase ($p<0.0001$), and GPx ($p<0.0001$).

The lipid peroxidation products like Malonaldehyde (MDA) and 4-Hydroxy Nonenal (4-HNE), is a measure of oxidative stress status. STZ and LPS induced significant ($P<0.0001$) increase in MDA levels compared to controls, the same thing was observed in case of 4-HNE. Treatment with UAEF significantly attenuated the elevation in MDA and 4-HNE levels (Figure 3.6 D and 3.6E) ($P<0.0001$). UAEF 50mg/Kg showed significantly ($P<0.0001$) marked reduction in MDA levels compared to low dose. Whereas, Metformin significantly attenuated elevated MDA and 4-HNE levels ($p<0.0001$) (figure3.6a and 3.6b).

Advanced glycation end products (AGEs) formation in DC rats was measured. Figure 5F demonstrated that AGEs levels were substantially elevated in DC group ($p<0.0001$). Different doses of UAEF 25mg/Kg and 50 mg/Kg and Metformin treatment significantly inhibited AGEs formation ($p<0.0001$).

Protein oxidation by several free radicals is the major factor in the development of diabetic cardiomyopathy. Protein oxidation products like protein carbonyls and thiols, AOPP were assessed in STZ and LPS induced and treated rats (Figure3.6). A significant ($P<0.0001$) increase in the levels of AOPP, protein carbonyls, and thiols (Figure3.6G, 3.6H, and 3.6I respectively) were observed in DC group compared to control. Therapy with UAEF significantly ($P<0.0001$) attenuated the protein carbonyls, thiols and AOPP. When compared to low dose, high dose (50mg/Kg) significantly reduced the protein carbonyls, thiols and AOPP. Metformin (100mg/Kg) substantially attenuated protein oxidation ($p<0.0001$)

3.7 UAEF restored mitochondria dysfunction and TCA enzymes in DCM rats.

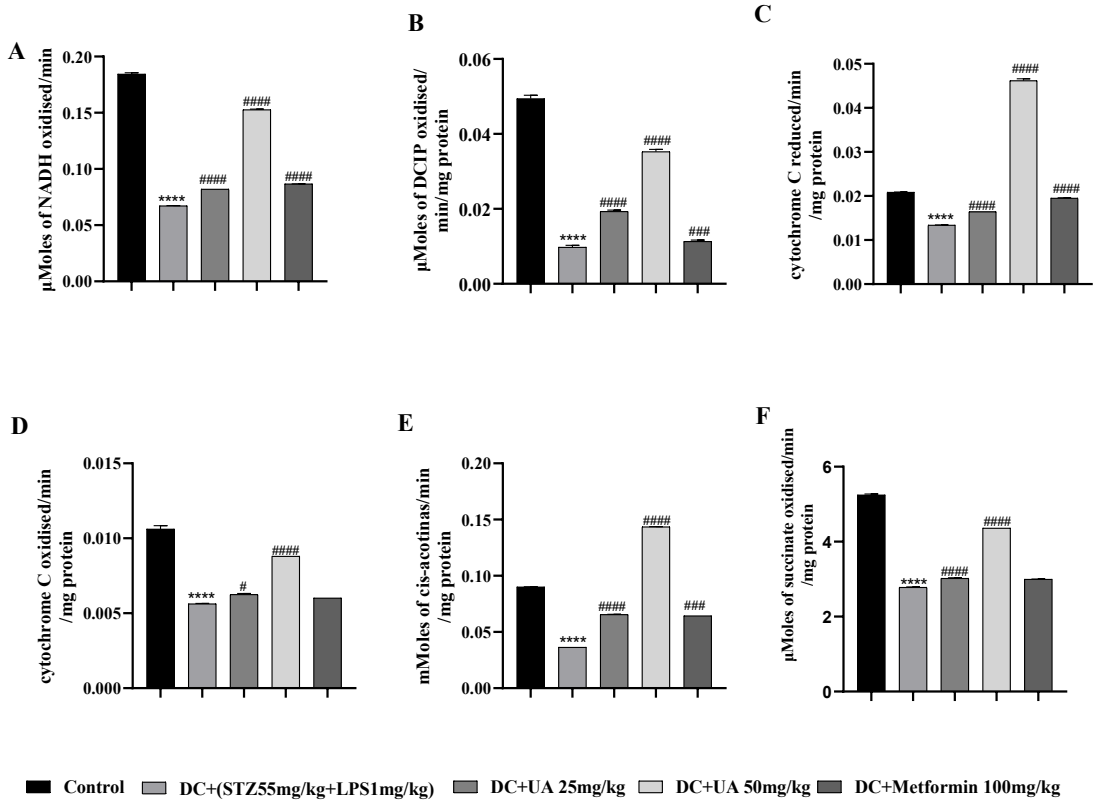


Figure 3.7: UAEF effect on mitochondrial complexes and TCA enzymes in DC rats.

DC rats were treated with different doses of UAEF 25 mg/Kg and 50 mg/Kg. After treatment period A) mitochondrial complex I, B) mitochondrial complex II, C) mitochondrial complex III, D) mitochondrial complex IV, E) aconitase, and F) SDH were measured in pooled heart homogenate using UV-Visible spectroscopic methods. Results were analyzed using one-way ANOVA, Tukey's multiple comparison post test. Values were expressed as mean±SEM, n=6. Whereas, $^{****}p<0.0001$, $^{**}p<0.0029$, $^{*}p<$ *vs* control and $^{\#\#\#\#}p<0.0001$, $^{\#\#\#}p<0.0001$, $^{\#\#}p<0.0001$, $^{\#}p<0.0001$ *vs* DCM

In DC, hyperglycaemia causes a reductive stress on mitochondrial complexes and alters mitochondrial membrane potential ultimately causing cardiac tissue injury. The present study was performed to determine the protective effect of UAEF on STZ and LPS induced mitochondrial dysfunction in heart tissue (Fig. 3.7). Our results have demonstrated that STZ and LPS induction reduced activity of complex I ($p<0.0019$), complex II ($p<0.0029$), Complex III ($p<0.0001$), and complex IV ($p<0.0001$) compared to the control group significantly (Figure 3.7A). UAEF (25 and 50 mg/Kg) treatment ($p<0.001$) improved complex activity more than the DC group (Fig. 3.7). However, 25 mg/kg UAEF treatment did not restore complex activity. However, 50 mg/Kg UAEF significantly enhanced complex I, Complex II ($p<0.0004$), complex III ($p<0.0395$), and complex IV ($p<0.0006$). Metformin (100 mg/Kg) substantially

increased the activities of complex I ($p<0.0001$) and complex IV ($p<0.0001$). TCA enzymes aconitase and Succinate Dehydrogenase (SDH) levels were significantly attenuated with STZ+LPS induction compared with the control group ($p<0.0001$). UAEF 25 and 50mg/kg treatment strengthened the activity of aconitase and SDH; the high dose (50mg/Kg) displayed pronounced improvement in aconitase ($p<0.0001$) and SDH ($p<0.0001$). Metformin restored both enzymes substantially ($p<0.0001$).

3.8 UAEF modulated genes related to inflammation and pyroptosis in DC rats

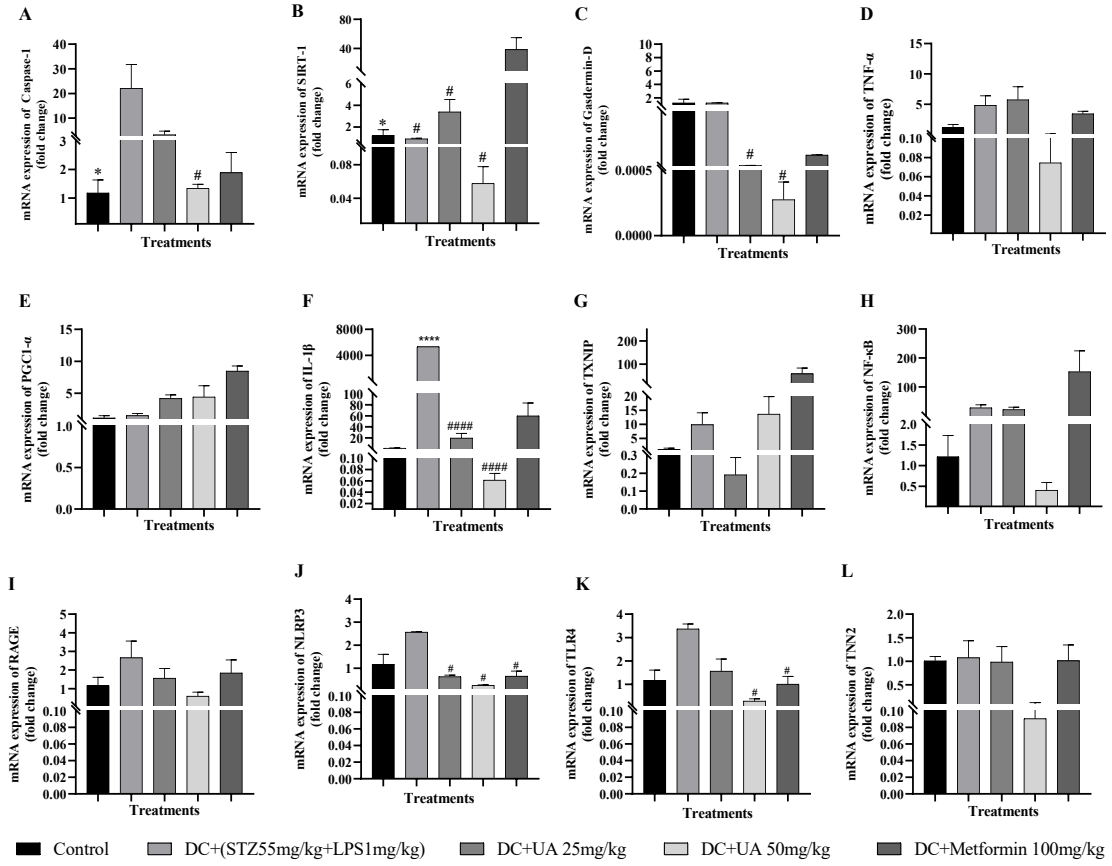


Figure 3.8: **Effect of UAEF on mRNA expression of metabolism, mitochondrial, inflammatory and Pyroptosis related genes in DC rats.**

Diabetic cardiomyopathy (DC) rats were treated with different doses UAEF 25mg/Kg and 50mg/Kg. After treatment period mRNA expression of genes A)Caspase-1, B) SIRT-1, C) Gasdermin-D, D) TNF-α, E)PGC1-α, F) IL-1β, G) TXNIP, H) NF-κB, I) RAGE, J) NLRP3, and K) TLR4, and L) TNNT2 were measured in pooled heart homogenate using RT-qPCR. Results were analyzed using one-way ANOVA, Tukey's multiple comparison post test. Values were expressed as mean±SEM, n=6. Whereas, $^{***}p<0.001$, $^{*}p<0.05$ *vs* control and $^{\#\#\#}p<0.001$, $^{\#\#}p<0.001$, $^{\#}p<0.05$ *vs* DC.

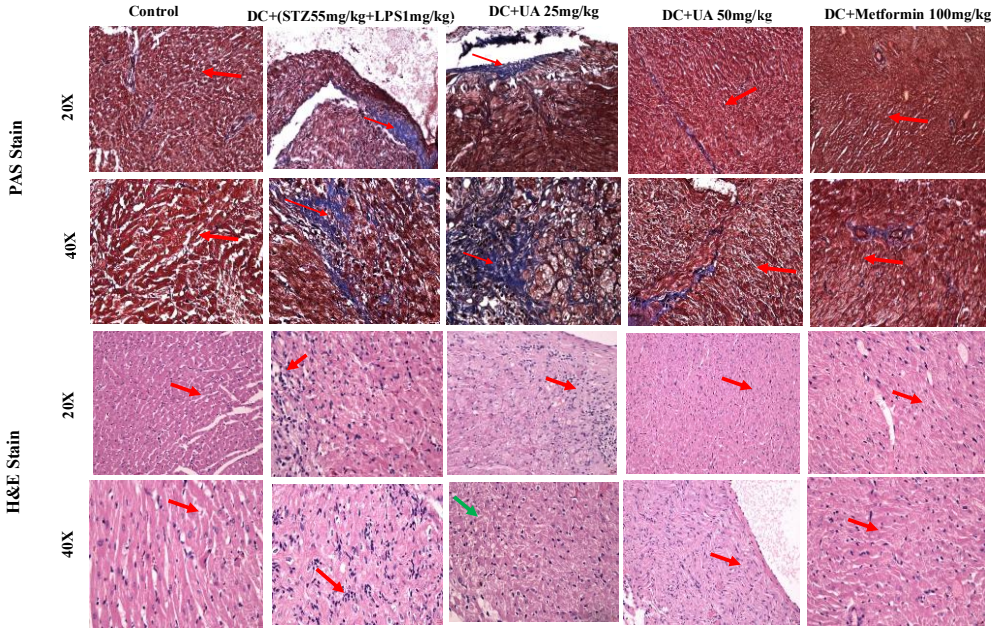
STZ-induced DC rats demonstrated significant upregulation of inflammatory mediators, including TNF-α ($p<0.001$), IL-1β ($p<0.001$), NF-κB ($p<0.001$), and RAGE ($p<0.045$)

compared to control group. Notably, UAEF treatment substantially decreased the expression of the inflammatory markers TNF-α ($p<0.001$), NF-κB ($p<0.001$), RAGE ($p<0.013$) than DC group (figure3.8). While Metformin also displayed significant attenuation ($p<0.001$). A profound elevation of Pyroptosis and inflammosome related genes like TXNIP, NLRP3, Caspase-1, and Gasdermin D expression ($p<0.0001$ vs control). UAEF and Metformin significantly ameliorated the expression of TXNIP (UAEF 25mg/Kg, $p<0.030$, and 50mg/Kg, $p<0.009$ vs DC group), NLRP3 (UAEF 25mg/Kg, $p<0.001$, and 50mg/Kg, $p<0.001$ vs DC group), Caspase-1(UAEF 25mg/Kg, $p<0.001$ vs DC group), and Gasdermin D (two doses of UAEF, $p<0.001$ vs DC group) (figure). DC group exhibited profound decrease in SIRT1 and PGC-1α ($p<0.001$) expression, reflecting impaired mitochondrial biogenesis, oxidative stress, and mitochondrial dysregulation in DC rats (figure). Treatment with UAEF and Metformin restored expression of genes significantly (SIRT1-$p<0.003$) than DCM group.

3.9 UAEF attenuated STZ and LPS induced histological changes in heart tissue

Fig. 3.9. Treatment with UAEF Substantially Suppresses the inflammation-Induced Histological Changes in Cardiac Tissues

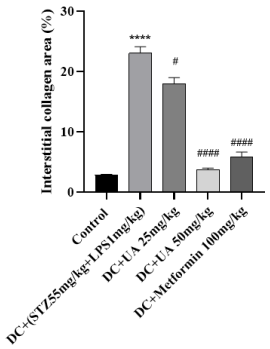
Animals were sacrificed, and the cardiac tissues were collected for histopathological studies. A) H&E staining, B) Masson trichrome staining. Images were acquired at 20× and 40× magnifications using a microscope (Scale bar: 100 µm). Histological scoring was done using a semi-quantitative scale: + (minimal), ++ (mild), +++ (moderate), and ++++ (marked). The grades reflected the extent of tissue alteration and inflammatory cell presence, fibroblasts proliferation, cardiomyocytes disarray, with minimal indicating <10 % involvement, mild 10–30 %, moderate 30–60 %, and marked >60 %. Scoring was performed in a blinded manner by an independent observer C) Quantification of inflammatory cellular infiltrates, cardiomyocyte degeneration, and collagen synthesis was represented. D) Quantification of interstitial collagen area (%) from Masson trichome staining using imageJ software. Significant differences



B

Characteristics	Control	DC group (STZ 55mg/kg+ LPS 1mg/Kg)	UAEF 25mg/Kg	UAEF 50 mg/Kg	Metformin 100mg/kg
Inflammatory cell infiltration	-	++++	++	-	-
Fibroblast proliferation and collagen deposition (green arrows)	-	++++	+++	+	-
Cardiomyocyte disarray (red arrows)	-	++++	+	-	-

C



between vehicle control and DC control were shown as ***p-values <0.001. Significant differences between the DC control and treatment groups were indicated by ###p < 0.001. Values of $^{\#\#}p < 0.01$, and $^{\#\#\#}p < 0.001$ were considered statistically significant compared with the UAEF treatment group.

Histopathological examination demonstrated substantial myocardial alterations in the STZ–LPS-induced diabetic cardiomyopathy (DC) group compared with the normal control group. H&E-stained sections of the control animals showed preserved myocardial architecture with regularly arranged cardiac muscle fibers and normal cellular morphology. In contrast, STZ–LPS administration resulted in marked disruption of myocardial architecture, myocyte degeneration, irregular arrangement of cardiac fibers, and increased cellular infiltration, indicating pronounced diabetes-associated cardiac injury (Figure 3.9A).

Treatment with the ursolic acid-enriched fraction (UAEF) attenuated these pathological alterations. The UAEF 25 mg/kg group showed partial restoration of myocardial architecture, with a reduction in myocyte degeneration and inflammatory cellular infiltration compared with the DC group. The UAEF 50 mg/kg group demonstrated a more pronounced improvement, characterized by relatively preserved myocardial fibers, reduced structural disruption, and decreased inflammatory changes (Figure 3.9B). The metformin-treated group (100 mg/kg) also exhibited substantial preservation of myocardial architecture, with histological features approaching those of the normal control group (figure 3.9C).

Masson's trichrome staining revealed increased collagen deposition in the DC group, suggesting enhanced myocardial fibrotic remodelling (figure 3.9A). UAEF treatment reduced the extent of collagen accumulation, with a greater reduction observed following 50 mg/kg UAEF compared with 25 mg/kg UAEF. The metformin group showed comparatively minimal collagen deposition and preserved myocardial architecture (figure 3.9A).

Overall, the histopathological findings indicate that UAEF exerted a dose-dependent cardioprotective effect against DC-induced myocardial injury and fibrotic remodeling, with 50 mg/kg UAEF producing a more pronounced protective response than 25 mg/kg UAEF. The effects observed with UAEF 50 mg/kg were comparable to those observed with the standard drug metformin 100mg/Kg.

4. Discussion

Diabetic cardiomyopathy (DCM) is a major cardiovascular complication of diabetes characterized by progressive myocardial structural and functional abnormalities in the absence of an overt primary cardiac disease. Chronic hyperglycemia, oxidative stress, mitochondrial

dysfunction, low-grade inflammation, advanced glycation end-product (AGE)-RAGE signaling, and activation of innate immune pathways collectively contribute to cardiomyocyte injury, myocardial remodeling, and fibrosis[6,7,8,9,16,17]. In the present study, we investigated the cardioprotective potential of a ursolic acid-enriched fraction (UAEF) in an experimental model of diabetic cardiomyopathy and explored its possible molecular mechanisms using biochemical, molecular, histopathological, network pharmacology, and molecular docking approaches.

The quantitative estimation of ursolic acid demonstrated successful enrichment of this triterpenoid in the prepared fraction (59.39±0.04). Standardization of the fraction based on its UA content provides an important chemical basis for interpreting the pharmacological effects observed in the present investigation ((figure 3.2). Ursolic acid has been reported to possess antioxidant, anti-inflammatory, metabolic, and cardioprotective properties [21–23,40], and its ability to influence multiple intracellular signaling pathways makes it a plausible bioactive constituent contributing to the observed effects of UAEF.

The diabetic model produced characteristic biochemical and molecular alterations consistent with cardiometabolic injury. Increased cardiac troponin levels indicate myocardial damage and provide evidence of cardiomyocyte membrane disruption in the diabetic condition (figure 3.8). The improvement in troponin levels following UAEF treatment suggests attenuation of diabetes-associated myocardial injury (figure3.5). This cardioprotective effect was further supported by the histopathological findings (figure 3.9), in which diabetic animals exhibited myocardial structural alterations, inflammatory changes, and increased extracellular matrix/collagen deposition, whereas UAEF treatment reduced these pathological changes (figure 3.9). The histological improvement indicates that the protective effect of UAEF extends beyond biochemical correction and involves preservation of myocardial architecture.

One of the important findings of the present study was the modulation of inflammatory mediators, particularly TNF-α and IL-1β (figure 3.8). Chronic hyperglycemia promotes oxidative and inflammatory stress within the myocardium, resulting in activation of inflammatory transcriptional pathways and release of pro-inflammatory cytokines. TNF-α and IL-1β can further aggravate cardiomyocyte dysfunction, oxidative stress, and mitochondrial injury, thereby establishing a self-amplifying inflammatory environment [17,18,67]. The reduction of these cytokines following UAEF treatment indicates suppression of diabetes-associated myocardial inflammation (figure 3.8). This effect may be particularly relevant

because persistent inflammation is increasingly recognized as an important driver of progression from metabolic stress to structural cardiac remodeling.

The present study further provides evidence for involvement of the NLRP3 inflammasome–caspase-1 pathway. NLRP3 activation represents an important mechanism linking metabolic stress, reactive oxygen species, mitochondrial dysfunction, and sterile inflammation [18,19,67,68]. Following activation, the NLRP3 inflammasome promotes caspase-1 activation, which facilitates maturation of IL-1β and contributes to inflammatory cell death through pyroptosis. The increased expression of NLRP3 and caspase-1 in diabetic cardiac tissue, together with elevation of IL-1β, suggests activation of inflammasome-associated inflammatory signaling in the diabetic myocardium (figure 3.8). The suppression of these alterations by UAEF indicates that the fraction may interfere with inflammasome activation and thereby reduce downstream inflammatory injury (figure 3.8).

Importantly, gasdermin D provides a mechanistic link between inflammasome activation and pyroptotic cell death. Activated caspase-1 cleaves gasdermin D, releasing its pore-forming N-terminal domain, which promotes plasma membrane pore formation and ultimately pyroptotic cell death[18,19,67,68]. Therefore, modulation of gasdermin D together with NLRP3, caspase-1, and IL-1β strengthens the interpretation that UAEF may suppress pyroptosis-associated myocardial injury rather than merely reducing nonspecific inflammation. The coordinated regulation of these components suggests that UAEF may interrupt the NLRP3/caspase-1/gasdermin D axis at multiple levels (figure 3.8).

The observed effects may also be associated with attenuation of the TLR4/NF-κB inflammatory genes. TLR4 acts as an important innate immune receptor capable of sensing endogenous danger-associated signals generated during metabolic stress. Its activation can stimulate downstream NF-κB signaling, resulting in transcription of inflammatory mediators, including TNF-α and pro-IL-1β [13,15,16,17]. Increased TLR4 and NF-κB signaling in diabetes may therefore provide an upstream stimulus for persistent myocardial inflammation and inflammasome activation [16,17,38,39]. The reduction of TLR4/NF-κB genes following UAEF administration suggests that the fraction may suppress upstream inflammatory activation, which could subsequently limit NLRP3 inflammasome priming and cytokine production (figure 3.8).

TXNIP may represent another important gene connection between oxidative stress and NLRP3 inflammasome activation. Diabetes-associated oxidative stress can promote TXNIP activation, and TXNIP has been implicated in the regulation of NLRP3 inflammasome signaling [19].

Thus, increased TXNIP expression may provide a molecular link between excessive reactive oxygen species and inflammatory activation in diabetic cardiomyopathy. The observed reduction in TXNIP following UAEF treatment suggests that attenuation of oxidative stress-related signaling may contribute to suppression of NLRP3 activation (figure 3.8). Collectively, the TLR4/NF-κB/TXNIP/NLRP3 axis provides a plausible mechanistic framework through which UAEF may reduce chronic inflammatory and pyroptotic responses in diabetic myocardium.

Another important aspect of DCM is mitochondrial dysfunction. The myocardium has a high energy requirement and is therefore particularly dependent on efficient mitochondrial oxidative metabolism [7,9,40]. Persistent hyperglycemia and oxidative stress can impair mitochondrial function, alter energy metabolism, and increase mitochondrial reactive oxygen species production. PGC-1α and SIRT1 are important regulators of mitochondrial biogenesis, oxidative metabolism, and cellular energy homeostasis. The observed restoration of PGC-1α and SIRT1 following UAEF treatment suggests improvement of mitochondrial regulatory mechanisms (figure 3.8). Activation of the SIRT1/PGC-1α axis may enhance mitochondrial biogenesis and oxidative capacity, thereby reducing metabolic stress within cardiomyocytes.

The interaction between mitochondrial dysfunction and inflammasome activation may be particularly important in the present model[19]. Damaged or dysfunctional mitochondria can generate excessive reactive oxygen species and release danger-associated signals capable of promoting NLRP3 inflammasome activation. Conversely, persistent inflammation can further impair mitochondrial function, creating a vicious cycle of oxidative stress, inflammation, and cardiomyocyte injury. By simultaneously improving SIRT1/PGC-1α-associated mitochondrial regulation and suppressing TXNIP/NLRP3-associated inflammatory genes, UAEF may interrupt this pathological loop (figure 3.8). This integratctivityed a may explain the broad cardioprotective effects observed in the present study.

AGE-RAGE signaling may provide an additional upstream mechanism contributing to the observed diabetic cardiac abnormalities. Chronic hyperglycemia promotes formation and accumulation of advanced glycation end products, which interact with their receptor RAGE and activate downstream inflammatory and oxidative signaling pathways[3,4,7,9,40]. RAGE activation can stimulate NF-κB and promote sustained expression of inflammatory genes. Therefore, attenuation of RAGE-associated signaling by UAEF may contribute to reduced oxidative stress and inflammation in diabetic myocardium (figure 3.8). The potential

interaction between RAGE signaling and TLR4/NF-κB pathways further supports the concept that UAEF acts on interconnected rather than isolated molecular targets.

The histopathological findings provide important structural evidence supporting these molecular observations. Diabetes-associated myocardial injury is characterized by cardiomyocyte degeneration, inflammatory infiltration, interstitial alterations, and increased collagen accumulation. Excessive extracellular matrix deposition can lead to myocardial stiffness, impaired ventricular compliance, and progressive cardiac remodeling[7,9,40]. The reduction in collagen deposition and improvement in myocardial architecture following UAEF treatment suggest an antifibrotic component of its cardioprotective action (figure 3.9). This structural improvement, together with reduced troponin levels and modulation of inflammatory and pyroptotic markers, indicates that UAEF may protect the myocardium through complementary biochemical and molecular mechanisms.

The network pharmacology analysis further supports the multitarget nature of the observed pharmacological effects. The predicted interactions between UAEF-associated phytoconstituents and multiple diabetes- and cardiovascular disease-related targets indicate that the biological activity of the fraction is unlikely to depend on a single molecular target[31–37]. Enrichment of targets associated with inflammation, oxidative stress, apoptosis/pyroptosis, mitochondrial regulation, and metabolic signaling is consistent with the experimental findings. In particular, the identification of targets related to NLRP3, NF-κB, TLR4, RAGE, TXNIP, SIRT1, and PGC-1α provides a computational basis for the interconnected mechanism proposed from the in vivo findings (figure 3.3).

Molecular docking analysis provided additional support for the predicted interactions between the major phytoconstituents, particularly ursolic acid, and selected protein targets[41,42]. Favorable docking interactions with inflammation- and metabolism-associated targets suggest that UAEF constituents may directly influence key signaling proteins. Thus, the convergence between computational prediction and experimental molecular data strengthens the proposed mechanism of action of UAEF (Table 3.1).

Overall, the present findings suggest that the ursolic acid-enriched fraction exerts a multitarget cardioprotective effect against diabetic cardiomyopathy through coordinated regulation of inflammatory, inflammasome/pyroptotic, oxidative, mitochondrial, and metabolic genes and antioxidative enzymes. The integration of experimental findings with network pharmacology and molecular docking provides a systems-level explanation for the pharmacological activity of UAEF. Nevertheless, further studies involving direct protein-level validation,

pharmacokinetic characterization, target-specific inhibition, will be required to establish definitive molecular target engagement and to determine ursolic acid cardioprotective potential.

5. Conclusion

The current study demonstrated the cardioprotective potential of ursolic acid enriched fraction (UAEF) against diabetic cardiomyopathy. UAEF treatment improved glycemic control, oxidative stress status, mitochondrial enzyme activity, and cardiac histopathological changes. It normalized moreover the expression of inflammation and pyroptosis-related genes such as TNF-α, IL-1β, NF-κB, TXNIP, NLRP3, caspase-1, Gasdermin D, and SIRT1. This was also consistent with potential interactions with inflammatory signalling-related targets as suggested by network pharmacology and molecular docking. At the doses tested, protective effects of UAEF were more potent with 50 mg/kg than 25 mg/kg. key findings imply that UAEF may ameliorates diabetes-induced cardiac injury by multiple mechanisms, especially those mediated by oxidative stress and inflammation. Further mechanistic studies are required to elucidate its specific molecular mechanisms and therapeutic potential in diabetic cardiomyopathy.

6. Limitations and Future directions of the study

The limitations of the current study should be acknowledged. First, the molecular validation of the proposed TLR4/NF-κB/TXNIP–NLRP3 inflammasome signaling pathway was not undertaken. The RT-PCR results suggested changes in the expression of genes associated with inflammation and pyroptosis, but protein levels were not confirmed, and there was no experimental evidence to demonstrate inflammasome assembly and pyroptotic cell death. In addition, the network pharmacology and molecular docking results are predictive and need biochemical and functional validation to establish cause-effect relationships for direct action targets and mechanisms. The functional effects of UAEF were also not investigated in the present study; echocardiography, detailed hemodynamic assessment of cardiac functions, and investigations of drug pharmacokinetics, bioavailability, and toxicity are well known to not be carried out.

Functional evaluation of inflammasome activation and pyroptosis should be undertaken, and future studies should seek to validate the proposed molecular mechanisms by protein-level studies of TLR4, NF-κB, TXNIP, NLRP3, cleaved caspase-1, and gasdermin D. Specific

biochemical assays and gene silencing where possible would further delineate the specific molecular targets for the observed effects. Testing of pure ursolic acid and more stringent phytochemical profiling and standardization of UAEF would be rewarding for demarcation of specific phytoconstituents and synergistic effects. However, further preclinical studies on heart maturation, pharmacokinetic evaluation, optimization/methodology for dosing, bioavailability, and chronic toxicity will be required. Finally, independent validation and translational research with proper design are needed to assess the therapeutic potential of UAEF as a phytopharmaceutical candidate for treating diabetic cardiomyopathy.

AUTHOR CONTRIBUTION

AK&YB: Conceptualization, methodology, investigation, data curation, formal analysis, visualization, and writing original draft.
ST&KM: Conceptualization, methodology
AT&GM: Methodology, Data curation, Formal analysis

DR: Conceptualization, Investigation, Methodology, Supervision, Writing- review & editing
All authors: Reviewed and approved the final manuscript and agreed to be accountable for all aspects of the work.

DECLARATION

We declare that this manuscript is original and has not been published previously, nor is it under consideration for publication in any other journal. All authors have read and approved the final version of the manuscript and agree to its submission to Journal of Ethanopharmacology. The authors further declare that there are no competing interests related to this work.

FUNDING DECLARATION

This Research received no external funding.

Conflict of Interest

The authors declare **no conflict of interest**.

Data availability

All data supporting the findings of this study are available within the paper.

References

1. Sun H, Saeedi P, Karuranga S, Pinkepank M, Ogurtsova K, Duncan BB, Stein C, Basit A, Chan JC, Mbanya JC, Pavkov ME. IDF Diabetes Atlas: Global, regional and country-level diabetes prevalence estimates for 2021 and projections for 2045. Diabetes research and clinical practice. 2022 Jan 1;183:109119.
2. Cole JB, Florez JC. Genetics of diabetes mellitus and diabetes complications. Nature Reviews Nephrology. 2020 Jul;16(7):377-90.
3. Chen Y, Meng Z, Li Y, Liu S, Hu P, Luo E. Advanced glycation end products and reactive oxygen species: uncovering the potential role of ferroptosis in diabetic complications. Molecular Medicine. 2024 Sep 9;30(1):141.
4. Chen X, Xie N, Feng L, Huang Y, Wu Y, Zhu H, Tang J, Zhang Y. Oxidative stress in diabetes mellitus and its complications: From pathophysiology to therapeutic strategies. Chinese Medical Journal. 2025 Jan 5;138(1):15-27.
5. Kalyani RR, Everett BM, Perreault L, Michos ED. Heart disease and diabetes. Diabetes in America [Internet]. 2023 Dec 20.
6. Jia G, Whaley-Connell A, Sowers JR. Diabetic cardiomyopathy: a hyperglycaemia-and insulin-resistance-induced heart disease. Diabetologia. 2018 Jan;61(1):21-8.
7. Tan Y, Zhang Z, Zheng C, Wintergerst KA, Keller BB, Cai L. Mechanisms of diabetic cardiomyopathy and potential therapeutic strategies: preclinical and clinical evidence. Nature Reviews Cardiology. 2020 Sep;17(9):585-607.
8. Dillmann WH. Diabetic cardiomyopathy: what is it and can it be fixed?. Circulation research. 2019 Apr 12;124(8):1160-2.
9. Huo JL, Feng Q, Pan S, Fu WJ, Liu Z, Liu Z. Diabetic cardiomyopathy: Early diagnostic biomarkers, pathogenetic mechanisms, and therapeutic interventions. Cell death discovery. 2023 Jul 21;9(1):256.

10. Lee JY, Bays DJ, Savage HP, Bäumler AJ. The human gut microbiome in health and disease: time for a new chapter?. Infection and Immunity. 2024 Nov 12;92(11):e00302-24.

11. Ghosh SS, Wang J, Yannie PJ, Ghosh S. Intestinal barrier dysfunction, LPS translocation, and disease development. Journal of the Endocrine Society. 2020 Feb;4(2):bvz039.

12. Violi F, Cammisotto V, Bartimoccia S, Pignatelli P, Carnevale R, Nocella C. Gut-derived low-grade endotoxaemia, atherothrombosis and cardiovascular disease. Nature Reviews Cardiology. 2023 Jan;20(1):24-37.

13. Stierschneider A, Wiesner C. Shedding light on the molecular and regulatory mechanisms of TLR4 signaling in endothelial cells under physiological and inflamed conditions. Frontiers in Immunology. 2023 Nov 24;14:1264889.

14. Oikonomou I, Papageorgiou A, de Lastic AL, Moulias A, Georgopoulou GA, Mouzaki A, Koufou EE, Tsigkas G, Gogos C, Davlouros P, Assimakopoulos SF. Gut barrier dysfunction, endotoxemia and inflammatory response in STEMI patients and effect of primary PCI. The American Journal of the Medical Sciences. 2024 Nov 1;368(5):485-93.

15. Oda M, Yamamoto H, Kawakami T. Maintenance of homeostasis by TLR4 ligands. Frontiers in immunology. 2024 Apr 23;15:1286270.

16. Liu HJ, Gui LK, Wei H, Zhou XY, Liu ZL, Jin LJ. The role of NF-κB in diabetic cardiomyopathy. All Life. 2024 Dec 31;17(1):2397402.

17. Ramesh P, Yeo JL, Brady EM, McCann GP. Role of inflammation in diabetic cardiomyopathy. Therapeutic Advances in Endocrinology and Metabolism. 2022 Mar;13:20420188221083530.

18. Lu Y, Lu Y, Meng J, Wang Z. Pyroptosis and its regulation in diabetic cardiomyop athy. Frontiers in Physiology. 2022 Jan 25;12:791848.

19. Swanson KV, Deng M, Ting JP. The NLRP3 inflammasome: molecular activation and regulation to therapeutics. Nature Reviews Immunology. 2019 Aug;19(8):477-89.

20. Liu HJ, Gui LK, Wei H, Zhou XY, Liu ZL, Jin LJ. The role of NF-κB in diabetic cardiomyopathy. All Life. 2024 Dec 31;17(1):2397402.

21. Cargnin ST, Gnoatto SB. Ursolic acid-enriched fraction from apple pomace and traditional plants: A valuable triterpenoid with functional properties. Food Chemistry. 2017 Apr 1;220:477-89.

22. Bakry SM, El-Shiekh RA, Hatem S, Mandour AA, El-Dessouki AM, Bishr A, Elosaily H, Mohamed AF, Elhusseiny SM. Therapeutic applications of Ursolic acid-enriched fraction: a comprehensive review and utilization of predictive tools. Future Journal of Pharmaceutical Sciences. 2025 Apr 22;11(1):48.

23. Zhao M, Wu F, Tang Z, Yang X, Liu Y, Wang F, Chen B. Anti-inflammatory and antioxidant activity of Ursolic acid-enriched fraction: a systematic review and meta-analysis. Frontiers in Pharmacology. 2023 Sep 28;14:1256946.

24. Jia Y, Kim S, Kim J, Kim B, Wu C, Lee JH, Jun HJ, Kim N, Lee D, Lee SJ. Ursolic acid-enriched fraction improves lipid and glucose metabolism in high-fat-fed C57BL/6J mice by activating peroxisome proliferator-activated receptor alpha and hepatic autophagy. Molecular nutrition & food research. 2015 Feb;59(2):344-54.

25. Ramírez-Rodríguez AM, González-Ortiz M, Martínez-Abundis E, Acuña Ortega N. Effect of Ursolic acid-enriched fraction on metabolic syndrome, insulin sensitivity, and inflammation. Journal of Medicinal Food. 2017 Sep;20(9):882-6.

26. Wang XT, Gong Y, Zhou B, Yang JJ, Cheng Y, Zhao JG, Qi MY. Ursolic acid-enriched fraction ameliorates oxidative stress, inflammation and fibrosis in diabetic cardiomyopathy rats. Biomedicine & Pharma.

27. Patel VS, Patel RC, Rathod DK, Patel SM, Rout SK. Development and validation of RP-HPLC method for determination of ursolic acid in Ocimum sanctum Linn in human plasma. Res. Educ. Indian Med. 2012;18(3-4):141.

28. Khanvilkar VV, Mandle SS, Hande PR, Daka BR, Jadhav PP. RP-HPLC method development and validation for simultaneous estimation of berberine and ursolic acid in formulation. Journal of Chromatographic Science. 2025 Apr;63(4):bmaf016.

29. Taralkar SV, Chattopadhyay S. A HPLC method for determination of ursolic acid and betulinic acids from their methanolic extracts of Vitex negundo Linn. J. Anal. Bioanal. Tech. 2012;3(3):1-6.

30. Kundu S, Selvaraj R, Reddy K, Vikram PR H, Gurupadayya B. Determination of ursolic acid in ethanolic extract of Rotheca serrata (L.) Steane & Mabb. by HPLC method. Natural Product Research. 2026 Jan 2;40(1):243-9.

31. Daina A, Michielin O, Zoete V. SwissTargetPrediction: updated data and new features for efficient prediction of protein targets of small molecules. Nucleic acids research. 2019 Jul 2;47(W1):W357-64.

32. Keiser MJ, Roth BL, Armbruster BN, Ernsberger P, Irwin JJ, Shoichet BK. Relating protein pharmacology by ligand chemistry. Nature biotechnology. 2007 Feb;25(2):197-206.

33. Stelzer G, Rosen N, Plaschkes I, Zimmerman S, Twik M, Fishilevich S, Stein TI, Nudel R, Lieder I, Mazor Y, Kaplan S. The GeneCards suite: from gene data mining to disease genome sequence analyses. Current protocols in bioinformatics. 2016 Jun;54(1):1-30.

34. Szklarczyk D, Gable AL, Nastou KC, Lyon D, Kirsch R, Pyysalo S, Doncheva NT, Legeay M, Fang T, Bork P, Jensen LJ. The STRING database in 2021: customizable protein–protein networks, and functional characterization of user-uploaded gene/measurement sets. Nucleic acids research. 2021 Jan 8;49(D1):D605-12.

35. Shannon P, Markiel A, Ozier O, Baliga NS, Wang JT, Ramage D, Amin N, Schwikowski B, Ideker T. Cytoscape: a software environment for integrated models of biomolecular interaction networks. Genome research. 2003 Nov;13(11):2498-504.

36. Sherman BT, Hao M, Qiu J, Jiao X, Baseler MW, Lane HC, Imamichi T, Chang W. DAVID: a web server for functional enrichment analysis and functional annotation of gene lists (2021 update). Nucleic acids research. 2022 Jul 5;50(W1):W216-21.

37. Kanehisa M, Furumichi M, Sato Y, Kawashima M, Ishiguro-Watanabe M. KEGG for taxonomy-based analysis of pathways and genomes. Nucleic acids research. 2023 Jan 6;51(D1):D587-92.

38. Zhao X, Zhang J, Xu F, Shang L, Liu Q, Shen C. TAK-242 alleviates diabetic cardiomyopathy via inhibiting pyroptosis and TLR4/CaMKII/NLRP3 pathway. Open Life Sciences. 2024 Sep 10;19(1):20220957.

39. Zhou X, Xing S, Zhang L, Lu J, Li D, Wang Y, Ma Y, Chang W, Su M. Amniotic mesenchymal stem cells attenuate diabetic cardiomyopathy by inhibiting pyroptosis via

modulation of the TLR4/NF-κb/NLRP3 pathway. Frontiers in Cell and Developmental Biology. 2025 Jul 10;13:1631973.

40. Wang XT, Gong Y, Zhou B, Yang JJ, Cheng Y, Zhao JG, Qi MY. Ursolic acid ameliorates oxidative stress, inflammation and fibrosis in diabetic cardiomyopathy rats. Biomedicine & Pharmacotherapy. 2018 Jan 1;97:1461-7.

41. Dallakyan S, Olson AJ. Small-molecule library screening by docking with PyRx. InChemical biology: methods and protocols 2014 Dec 22 (pp. 243-250). New York, NY: Springer New York.

42. Trott O, Olson AJ. AutoDock Vina: improving the speed and accuracy of docking with a new scoring function, efficient optimization, and multithreading. Journal of computational chemistry. 2010 Jan 30;31(2):455-61.

43. Chomczynski P. A reagent for the single-step simultaneous isolation of RNA, DNA and proteins from cell and tissue samples. Biotechniques. 1993 Sep 1;15(3):532-4.

44. Wang XT, Gong Y, Zhou B, Yang JJ, Cheng Y, Zhao JG, Qi MY. Ursolic acid ameliorates oxidative stress, inflammation and fibrosis in diabetic cardiomyopathy rats. Biomedicine & Pharmacotherapy. 2018 Jan 1;97:1461-7.

45. Ye J, Coulouris G, Zaretskaya I, Cutcutache I, Rozen S, Madden TL. Primer-BLAST: a tool to design target-specific primers for polymerase chain reaction. BMC bioinformatics. 2012 Jun 18;13(1):134.

46. Untergasser A, Cutcutache I, Koressaar T, Ye J, Faircloth BC, Remm M, Rozen SG. Primer3—new capabilities and interfaces. Nucleic acids research. 2012 Aug 1;40(15):e115-.

47. Halliwell B, Gutteridge JM, Aruoma OI. The deoxyribose method: a simple “test-tube” assay for determination of rate constants for reactions of hydroxyl radicals. Analytical biochemistry. 1987 Aug 15;165(1):215-9.

48. Beauchamp C, Fridovich I. Superoxide dismutase: improved assays and an assay applicable to acrylamide gels. Analytical biochemistry. 1971 Nov 1;44(1):276-87.

49. Marcocci L, Maguire JJ, Droylefaix MT, Packer L. The nitric oxide-scavenging properties of Ginkgo biloba extract EGb 761. Biochemical and biophysical research communications. 1994 Jun 15;201(2):748-55.

50. Thilavech T, Ngamukote S, Belobrajdic D, Abeywardena M, Adisakwattana S. Cyanidin-3-rutinoside attenuates methylglyoxal-induced protein glycation and DNA damage via carbonyl trapping ability and scavenging reactive oxygen species. BMC complementary and alternative medicine. 2016 May 23;16(1):138.

51. Singh H, Singh R, Singh A, Singh H, Singh G, Kaur S, Singh B. Role of oxidative stress in diabetes-induced complications and their management with antioxidants. Archives of Physiology and Biochemistry. 2024 Nov 1;130(6):616-41.

52. Furman BL. Streptozotocin-induced diabetic models in mice and rats. Current protocols in pharmacology. 2015 Sep;70(1):5-47.

53. Radhiga T, Rajamanickam C, Senthil S, Pugalendi KV. Effect of ursolic acid on cardiac marker enzymes, lipid profile and macroscopic enzyme mapping assay in isoproterenol-induced myocardial ischemic rats. Food and Chemical Toxicology. 2012 Nov 1;50(11):3971-7.

54. Ohkawa H, Ohishi N, Yagi K. Assay for lipid peroxides in animal tissues by thiobarbituric acid reaction. Analytical biochemistry. 1979 Jun 1;95(2):351-8.

55. Misra HP, Fridovich I. The role of superoxide anion in the autoxidation of epinephrine and a simple assay for superoxide dismutase. Journal of Biological chemistry. 1972 May 25;247(10):3170-5.

56. Szymonik-Lesiuk S, Czechowska G, Stryjecka-Zimmer M, Słomka M, MĄldro A, Celiński K, Wielosz M. Catalase, superoxide dismutase, and glutathione peroxidase activities in various rat tissues after carbon tetrachloride intoxication. Journal of hepato-biliary-pancreatic surgery. 2003 Aug;10(4):309-15.

57. Ellman GL. Tissue sulfhydryl groups. Archives of biochemistry and biophysics. 1959 May 1;82(1):70-7.

58. Paglia DE, Valentine WN. Studies on the quantitative and qualitative characterization of erythrocyte glutathione peroxidase. The Journal of laboratory and clinical medicine. 1967 Jul 1;70(1):158-69.

59. Witko-Sarsat V, Friedlander M, Capeillère-Blandin C, Nguyen-Khoa T, Nguyen AT, Zingraff J, Jungers P, Descamps-Latscha B. Advanced oxidation protein products as a novel marker of oxidative stress in uremia. Kidney international. 1996 May 1;49(5):1304-13.

60. Spinazzi M, Casarin A, Pertegato V, Salviati L, Angelini C. Assessment of mitochondrial respiratory chain enzymatic activities on tissues and cultured cells. Nature protocols. 2012 Jun;7(6):1235-46.

61. RJ P. Biochemistry of dystrophic muscle. Mitochondrial succinate-tetrazolium reductase and adenosine triphosphatase. The Biochemical Journal. 1961 Sep 1;80:649-54.

62. Gardner PR. Aconitase: sensitive target and measure of superoxide. InMethods in enzymology 2002 Jan 1 (Vol. 349, pp. 9-23). Academic Press.

63. Bradford MM. A rapid and sensitive method for the quantitation of microgram quantities of protein utilizing the principle of protein-dye binding. Analytical biochemistry. 1976 May 7;72(1-2):248-54.

64. Bancroft JD, Gamble M, editors. Theory and practice of histological techniques. Elsevier health sciences; 2008.

65. GoMori G. A rapid one-step trichrome stain. American journal of clinical pathology. 1950 Jul 1;20(7_ts):661-4.

66. McManus JF. Histological demonstration of mucin after periodic acid. Nature. 1946 Aug 10;158(4006):202-.